DUSP4 deficiency caused by promoter hypermethylation drives JNK signaling and tumor cell survival in diffuse large B cell lymphoma

Corina A. Schmid,[1] Mark D. Robinson,[2,3] Nicole A. Scheifinger,[1] Sebastian Müller,[4,5] Sergio Cogliatti,[6] Alexandar Tzankov,[7] and Anne Müller[1]

[1]Institute of Molecular Cancer Research, [2]Institute of Molecular Life Sciences, and [3]Swiss Institute of Bioinformatics (SIB), University of Zürich, 8057 Zürich, Switzerland
[4]Institute of Food, Nutrition, and Health and [5]Institute of Molecular Systems Biology, Swiss Federal Institute of Technology Zürich (ETHZ), 8093 Zürich, Switzerland
[6]Institute of Pathology, Cantonal Hospital of St. Gallen, 9007 St. Gallen, Switzerland
[7]Institute of Pathology, University Hospital Basel, 4031 Basel, Switzerland

The epigenetic dysregulation of tumor suppressor genes is an important driver of human carcinogenesis. We have combined genome-wide DNA methylation analyses and gene expression profiling after pharmacological DNA demethylation with functional screening to identify novel tumor suppressors in diffuse large B cell lymphoma (DLBCL). We find that a CpG island in the promoter of the dual-specificity phosphatase DUSP4 is aberrantly methylated in nodal and extranodal DLBCL, irrespective of ABC or GCB subtype, resulting in loss of DUSP4 expression in 75% of >200 examined cases. The *DUSP4* genomic locus is further deleted in up to 13% of aggressive B cell lymphomas, and the lack of DUSP4 is a negative prognostic factor in three independent cohorts of DLBCL patients. Ectopic expression of wild-type DUSP4, but not of a phosphatase-deficient mutant, dephosphorylates c-JUN N-terminal kinase (JNK) and induces apoptosis in DLBCL cells. Pharmacological or dominant-negative JNK inhibition restricts DLBCL survival in vitro and in vivo and synergizes strongly with the Bruton's tyrosine kinase inhibitor ibrutinib. Our results indicate that DLBCL cells depend on JNK signaling for survival. This finding provides a mechanistic basis for the clinical development of JNK inhibitors in DLBCL, ideally in synthetic lethal combinations with inhibitors of chronic active B cell receptor signaling.

CORRESPONDENCE
Anne Müller:
mueller@imcr.uzh.ch

Abbreviations used: BLBC, basal-like breast cancer; BTK, Bruton's tyrosine kinase; CLL, chronic lymphocytic leukemia; DLBCL, diffuse large B cell lymphoma; FFPE, formalin fixed, paraffin embedded; FL, follicular lymphoma; GC, germinal center; IHC, immunohistochemistry; MALT, mucosa-associated lymphoid tissue; MCL, mantle cell lymphoma; MZL, marginal zone lymphoma; PBA, 4-phenylbutyric acid; PI, propidium iodide; qRT-PCR, quantitative RT-PCR.

Diffuse large B cell lymphoma (DLBCL) is the most commonly diagnosed lymphoma in adults. It may either arise de novo at nodal or extranodal sites or as a consequence of malignant transformation of indolent lymphomas or leukemias such as follicular lymphoma (FL), chronic lymphocytic leukemia (CLL), and marginal zone lymphoma (MZL; Schneider et al., 2011; Shaffer et al., 2012; Pasqualucci and Dalla-Favera, 2014). DLBCL represents a heterogeneous disease, with molecular subtypes being characterized by distinct gene expression profiles, specific sets of somatic mutations, and differentially active intracellular signaling pathways (Roschewski et al., 2014). Three subtypes of DLBCL can be distinguished based on the presumed normal B cell counterpart, with activated B cell–like DLBCL (ABC-DLBCL) resembling the post–germinal center (GC) plasmablast, GC B cell–like DLBCL (GCB-DLBCL) deriving from GC B cells, and primary mediastinal B cell lymphoma (PMBL) arising in the thymus from a rare subset of thymic B cells (Alizadeh et al., 2000; Rosenwald et al., 2003). The three subtypes of DLBCL differ not only in their pathogenesis, but also in their cure and survival rates (Cultrera and Dalia, 2012). The rational development of more targeted therapies is complicated by the heterogeneity of DLBCL as well as

The Rockefeller University Press $30.00
J. Exp. Med. 2015
www.jem.org/cgi/doi/10.1084/jem.20141957

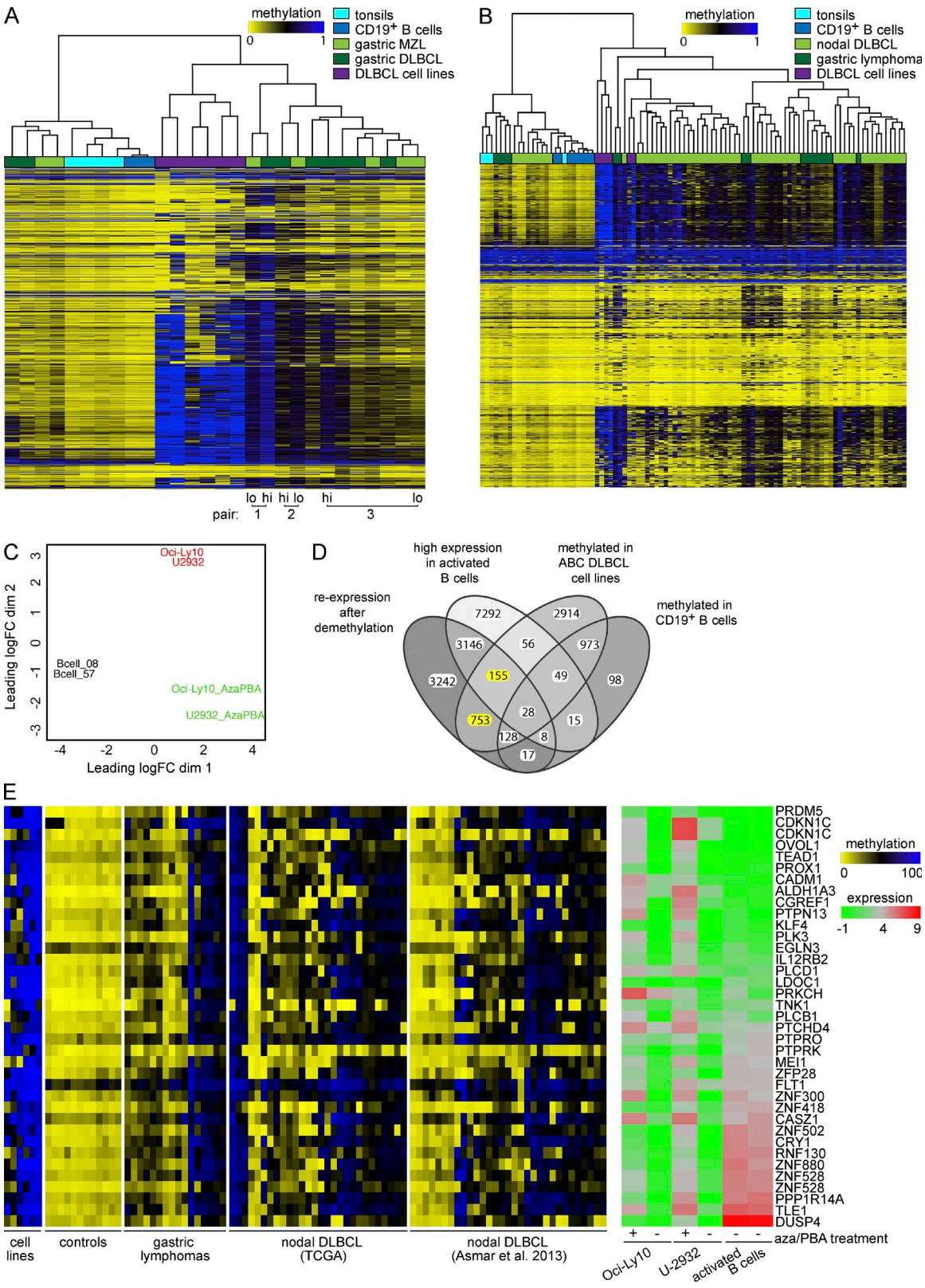

Figure 1. Integration of DNA methylation and RNA expression profiles identifies potential tumor suppressor genes in DLBCL. (A) The median methylation of CpG islands in promoter and regulatory regions was determined for 6 DLBCL cell lines (purple), 6 controls (tonsils and CD19+ B cells, light and dark blue), and 16 gastric lymphoma samples (MZL and DLBCL, light and dark green). Islands with a range in β values over all samples of at least 0.25 were used for hierarchical clustering (metric = 1-Spearman correlation, linkage = complete). Pairs of low (MZL)- and high-grade (DLBCL) samples obtained

the coexistence of genetic lesions affecting multiple redundant survival pathways. Genetic aberrations in DLBCL either exclusively affect GCB-DLBCL (deregulated c-Myc or Bcl-2 expression, gain of function of the H3K27 methyltransferase EZH2) or ABC-DLBCL (A20 loss, gain of function of MYD88, CD79A/B, or CARD11, all of which promote the constitutive activation of the NF-κB pathway) or are found in both major subtypes (inactivating mutations and deletions in the histone acetyltransferases CBP and p300 as well as the histone methyl transferase MLL2; Schneider et al., 2011; Shaffer et al., 2012; Pasqualucci and Dalla-Favera, 2014).

Aberrant changes of the DNA methylation landscape are a hallmark of cancer cells and have been linked to clinical aggressiveness and chemoresistance of DLBCL (Shaknovich et al., 2010; Clozel et al., 2013; De et al., 2013; Chambwe et al., 2014). Examples of tumor suppressor genes known to be silenced by promoter hypermethylation in DLBCL include *SMAD1*, *MGMT*, *CDKN2A*, and the *lamin A/C* gene (Martinez-Delgado et al., 1997; Esteller et al., 2002; Agrelo et al., 2005; Clozel et al., 2013). We have shown in earlier studies that the epigenetic silencing of the tumor suppressor microRNAs miR-203 and miR-34a contribute to the transformation of gastric MZL to DLBCL and to the deregulated expression of the hematopoietic oncoprotein FoxP1 (Craig et al., 2011a,b). Here, we have conducted a genome-wide analysis of the DNA methylome of gastric DLBCL and MZL and of nodal DLBCL samples and cell lines. The hypermethylated gene loci were further examined by RNA sequencing with respect to their reactivation upon experimental DNA demethylation. Aberrantly silenced genes were ectopically expressed in DLBCL cell lines and assessed for possible effects on cell survival. This unbiased approach uncovered a new tumor suppressor in DLBCL, the dual-specificity phosphatase DUSP4, and introduces the constitutively active JNK signaling pathway as a promising new target in DLBCL treatment.

RESULTS

Genome-wide profiling of DNA methylation and gene expression reveals epigenetic silencing of putative tumor suppressor genes in gastric and nodal DLBCL

To generate a global DNA methylation profile of gastric B cell lymphoma, we hybridized DNA from 16 archived paraffin-embedded lymphoma biopsies (7 MZL of mucosa-associated lymphoid tissue [MALT] type, 9 gastric DLBCL) and 6 DLBCL cell lines to human Methylation450BeadChip arrays. Four tonsil and two $CD19^+$ B cell samples served as normal controls. Unsupervised hierarchical clustering of all 28 samples revealed a promoter methylation signature that was shared by the majority of gastric lymphomas and DLBCL cell lines, but not the normal controls (Fig. 1 A). Gastric MZL and DLBCL exhibited largely indistinguishable methylation patterns, especially if taken sequentially from the same patient (Fig. 1 A). A comprehensive analysis integrating a published (Asmar et al., 2013) as well as a publicly accessible (Cancer Genome Atlas) dataset of nodal DLBCL with our gastric dataset revealed a shared DLBCL methylation signature irrespective of anatomical location (Fig. 1 B). To assess which of the aberrantly methylated genes could be transcriptionally reactivated by global DNA demethylation, we performed RNA sequencing of DLBCL cell lines before and after treatment with the demethylating agent 5-aza-2′-deoxycytidine in combination with the HDAC inhibitor 4-phenylbutyric acid (PBA) and of two human blood donor-derived B cell samples that had been activated in vitro by IgM and CD40 cross-linking. Principal component analysis revealed the segregation of the samples based on the experimental treatment they were subjected to (Fig. 1 C). We then integrated the information gleaned from the global DNA methylation and gene expression surveys to identify genes that (a) are re-expressed upon DNA demethylation, (b) are aberrantly methylated in the cell lines, and (c) are either expressed or not in normal B cells activated in vitro. Of the ∼900 genes identified by this approach (Fig. 1 D), 35 were found to be hypermethylated also in a majority of the 16 gastric and 59 nodal lymphoma samples (Fig. 1 E). Several of these genes had previously been described to be epigenetically regulated in B cell lymphomas, i.e., CDKN1C (Li et al., 2002), KLF4 (Guan et al., 2010), and TLE-1 (Fraga et al., 2008).

We were able to obtain expression constructs for 30 of the 35 genes of interest for the functional assessment of their tumor-suppressive properties. The ectopic expression of 8 of the 30 genes strongly and consistently reduced the viability of two DLBCL cells lines as assessed by metabolic activity assay and annexin V staining of apoptotic cells (Fig. 2, A and B). All eight genes thus likely represent epigenetically silenced tumor suppressor genes in DLBCL (see Fig. 2 C for their methylation status in the clinical samples and cell lines); of

from the same patient are indicated ($n = 3$). (B) Hierarchical clustering based on CpG island methylation in promoter and regulatory regions of the samples shown in A, along with 6 additional B cell samples (blue) and 59 nodal DLBCL cases (light green). (C) Multidimensional scaling (MDS) plot highlighting the overall similarity in gene expression levels, as determined by RNA sequencing and principal component analysis, of the six indicated samples in two-dimensional representation. The distances between samples represent the estimates of the coefficient of variation of expression between samples for the top 500 most variable genes. (D) Venn diagram of methylated and expressed genes as classified based on the following four outcomes (from left): (a) differentially expressed in DLBCL cell lines before and after 5-aza-2′-deoxycytidine and PBA treatment, FDR of 5%; (b) highly expressed in activated B cells, according to a selected cut-off separating the two modes of the expression distribution, in log (counts per million); (c) methylated (β value >0.6) in at least two out of three ABC-DLBCL cell lines; (d) methylated (β value >0.6) in $CD19^+$ B cells. Gene groups of interest are highlighted in yellow. (E) Methylation and expression data for 35 selected candidate genes (names indicated on the right) are shown. The yellow–black–blue color scale shows median CpG island β values for gastric lymphomas ($n = 16$), DLBCL cell lines ($n = 6$), normal controls ($n = 12$), and nodal DLBCL samples ($n = 59$); the green–gray–red color scale shows log (counts per million) expression values for activated B cells and DLBCL cell lines ($n = 2$; the results represent a limited number of repeats) before and after 5-aza-2′-deoxycytidine and PBA treatment.

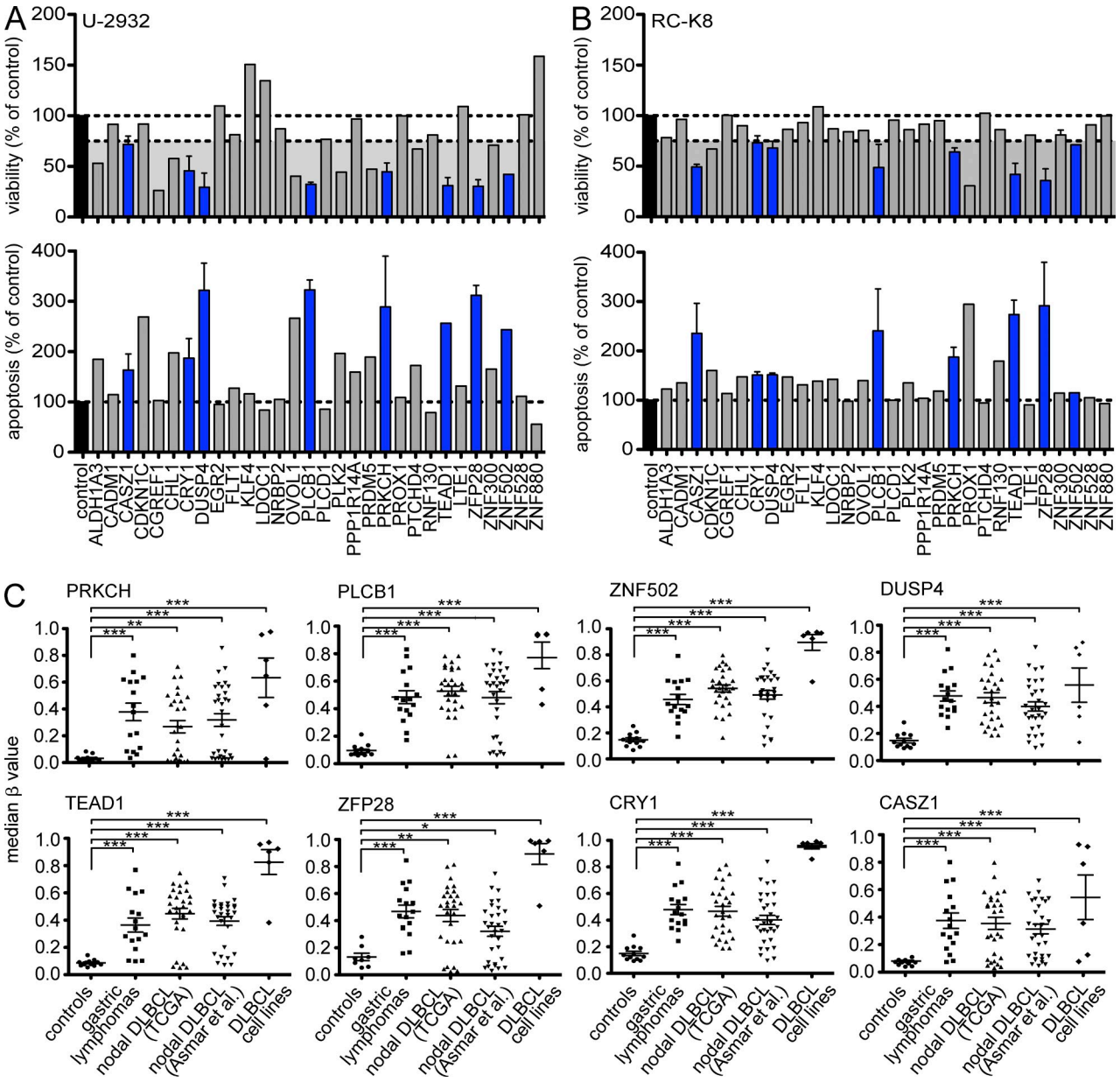

Figure 2. Eight epigenetically silenced genes are proapoptotic in DLBCL cell lines. (A and B) Functional analysis was conducted of 30 candidate genes in U-2932 (A) and RC-K8 (B) cell lines. Cell viability and apoptosis were assessed 72 h after electroporation with the indicated expression plasmids by CellTiter-Blue assay and annexin V staining, respectively (top and bottom panels), and are represented relative to empty vector–transfected controls. A second round of experiments was performed with candidates that reduced the viability below 75% of controls in both cell lines (blue bars; mean + SEM of two independent experiments; the results represent a limited number of repeats). (C) Median β values were calculated for all probes corresponding to the regulatory and promoter regions of the eight genes with proapoptotic activity identified in A and B, as determined by methylation array for the indicated samples (mean ± SEM). *, $P < 0.05$; **, $P < 0.01$; ***, $P < 0.001$, two-tailed Student's *t* test.

the eight, five encode transcription factors (*CRY1*, *CASZ1*, *ZNF502*, *TEAD1*, and *ZFP28*), and the remaining three encode proteins with enzymatic activity (the phosphatase *DUSP4*, the kinase *PRKCH*, and the phospholipase C β1 *PLCB1*). None of the eight genes have been functionally linked to the pathogenesis of DLBCL or any other type of B cell lymphoma, although two have been implicated in other hematological malignancies (*CRY1* in CLL; *PLCB1* in myelodysplastic syndrome).

The *DUSP4* genomic locus is hypermethylated or deleted in nodal and extranodal DLBCL

We focused on the dual-specificity phosphatase DUSP4 in all subsequent experimental efforts because it showed the highest expression in normal activated B cells and was strongly reactivated upon 5-aza-2′-deoxycytidine and PBA treatment in U2932 cells (Fig. 1 E; note that the other investigated cell line, Oci-Ly10, carries a deletion in one of two *DUSP4* alleles, which attenuates the ability of this cell line to up-regulate

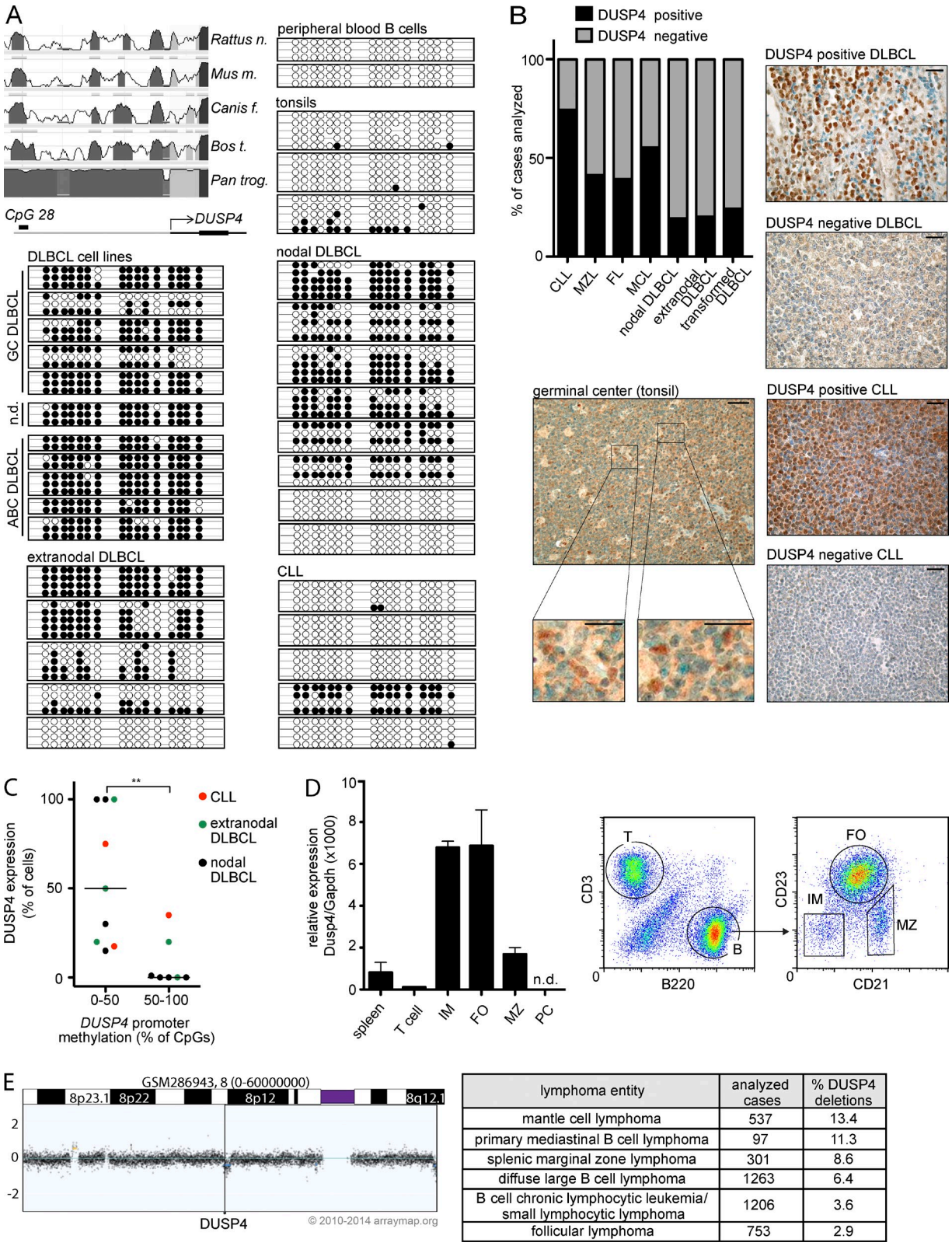

lymphoma entity	analyzed cases	% DUSP4 deletions
mantle cell lymphoma	537	13.4
primary mediastinal B cell lymphoma	97	11.3
splenic marginal zone lymphoma	301	8.6
diffuse large B cell lymphoma	1263	6.4
B cell chronic lymphocytic leukemia/ small lymphocytic lymphoma	1206	3.6
follicular lymphoma	753	2.9

Figure 3. The *DUSP4* promoter is hypermethylated in nodal and extranodal DLBCL, which correlates with lack of DUSP4 protein expression. (A) Bisulfite sequencing of 16 CpG dinucleotides in island 28 was performed for 11 DLBCL cell lines and 2 peripheral blood B cell samples and a set of 18 clinical lymphoma and 3 tonsil samples. Closed and open circles represent methylated and unmethylated CpGs, respectively. Between two and five clones were sequenced per sample. The alignment of the *DUSP4* promoter sequence of the indicated species was performed using ECR Browser and shows the high

DUSP4 upon 5-aza-2′-deoxycytidine and PBA treatment) and because the signaling pathways targeted by DUSP4 appeared likely to contribute to DLBCL pathogenesis. To validate our methylation array–based findings on a separate set of DLBCL samples using a different technical approach, we performed bisulfite sequencing of the CpG island 28 upstream of the *DUSP4* transcription start site (Waha et al., 2010). All 11 examined cell lines and 10 of 13 primary nodal and extranodal DLBCL patient biopsies exhibited widespread *DUSP4* promoter methylation, whereas normal B cells and tonsil samples were unmethylated (Fig. 3 A). Aberrant methylation of the *DUSP4* locus is thus a unifying feature of DLBCL irrespective of the subtype and anatomical site of origin, but was not observed in CLL (Fig. 3 A). Preliminary data obtained by chromatin immunoprecipitation of various epigenetically modified histone variants followed by PCR-based amplification of the *DUSP4* CpG island 28 suggest that repressive histone marks (H3K9me2, H3K27me3) are enriched and active histone marks (H3K9ac, H4ac) are underrepresented at the *DUSP4* promoter in the DLBCL cell line SU-DHL16 relative to normal blood-derived B cells (not depicted). To examine whether promoter hypermethylation and repressive histone modifications at the *DUSP4* promoter indeed result in loss of DUSP4 expression, we performed DUSP4-specific immunohistochemistry (IHC) on a B cell lymphoma tissue microarray featuring 397 cases that range in aggressiveness from indolent MZL of MALT type to primary nodal, extranodal, and secondary transformed DLBCL; several tonsil samples were examined for comparison. DUSP4 expression was exclusively nuclear in all DUSP4-positive cells (Fig. 3 B). Individual positive cells were detectable in the GCs of tonsils (Fig. 3 B). Interestingly, whereas 42% of MZL, 75% of CLL, 40% of FLs, and 56% of mantle cell lymphomas (MCLs) were positive for DUSP4 expression, that rate dropped to 20–25% for high-grade transformed DLBCL originating from gastric MZLs, FLs, or CLL (Fig. 3 B). Primary nodal and extranodal DLBCL had similar low rates of DUSP4 positivity. Whereas DUSP4 expression rates were thus significantly different between aggressive and indolent lymphomas ($P = 0.01$), no significant differences could be detected between the classified cases of ABC (26 of 83; 31%)- and GCB-type (11 of 33; 33%) nodal DLBCL. We further performed both DUSP4 IHC and bisulfite sequencing of 16 cases of DLBCL and CLL and indeed found a clear inverse association between DUSP4 expression and the extent of *DUSP4* promoter methylation (Fig. 3 C). To examine in more detail which lymphocyte subsets express DUSP4 under physiological conditions, we sorted $CD138^+$ plasma cells from mouse bone marrow and various lymphocyte subsets from mouse spleen. Interestingly, expression of DUSP4 was limited to splenic follicular and immature B cells and was not found in plasma cells, splenic marginal zone B cells, or splenic T cells (Fig. 3 D).

We next examined whether the *DUSP4* genomic locus is subject to recurrent deletion events. Of the 1,263 DLBCL samples for which comparative genomic hybridization data are available from a publicly accessible database of DNA copy number alterations (http://www.progenetix.org; Baudis and Cleary, 2001), 6.4% exhibited losses in the *DUSP4* genomic locus, of which a few were highly focal (Fig. 3 E). The fractions of other B cell lymphoma and leukemia entities with *DUSP4* deletions ranged from 3% (CLL and FL) to 13.4% (MCL; Fig. 3 E). In conclusion, loss of DUSP4 expression is a common event in lymphomagenesis and can be attributed either to the relatively rare loss of the *DUSP4* genomic locus or to its commonly observed epigenetic modification.

DUSP4 promoter hypermethylation represses DUSP4 expression

To experimentally assess whether *DUSP4* promoter hypermethylation affects DUSP4 expression, we first examined DUSP4 levels in blood-derived B cells from healthy human donors. Circulating human B cells with unmethylated *DUSP4* promoters (Fig. 3 A) did not express DUSP4 unless they were activated by IgM and/or CD40 cross-linking or treatment with the phorbol ester PMA (Fig. 4 A), an analogue of diacylglycerol which stimulates protein kinase C–dependent B cell activation (Teixeira et al., 2003; Cagnol and Rivard, 2013). In contrast, DLBCL cell lines with hypermethylated promoters failed to optimally express DUSP4 even when treated with PMA, unless they had been subjected to prior treatment with 5-aza-2′-deoxycytidine in combination with the HDAC inhibitor PBA (Fig. 4, B and C). Similarly, treatment with an IgM cross-linking antibody activated optimal DUSP4 expression in

conservation of CpG island 28 in other mammalian species relative to the human sequence (top left). (B) DUSP4 expression by the indicated lymphoma entities was assessed by IHC of a lymphoma tissue microarray. The graph shows percentage of DUSP4-positive cases (>30% positive cells) and DUSP4-negative cases (<30% positive cells) for the indicated lymphoma entities (top left). Representative micrographs show staining of a tonsillar GC (with insets) as well as DUSP4-positive and -negative DLBCL and CLL cases (bars, 50 µm; insets bars, 25 µm). CLL, $n = 20$; MZL, $n = 54$; FL, $n = 48$; MCL, $n = 9$; nodal DLBCL, $n = 170$; extranodal DLBCL, $n = 87$; transformed DLBCL, $n = 9$; and tonsils, $n = 3$. (C) The correlation of *DUSP4* promoter methylation (assessed by bisulfite sequencing) with DUSP4 protein expression (determined by IHC) was plotted for 16 lymphoma cases. **, $P < 0.01$, calculated using Mann–Whitney test; horizontal lines indicate medians. (D) $CD138^+$ plasma cells were isolated from 9-mo-old C57BL/6 mice. T cells and B cell subsets were sorted from splenocyte preparations based on CD3, B220, CD21, and CD23 expression according to the depicted sorting strategy. DUSP4 expression in the indicated subsets was analyzed by qRT-PCR and depicted as mean + SEM. Plasma cells: two pools of three mice each; T cells: $n = 2$ individual mice (the results represent a limited number of repeats); spleen: $n = 3$ individual mice; IM, MZ, and FO: $n = 5$ individual mice. n.d., not detected; T, T cells; B, B cells; IM, immature splenic B cells ($CD21^{low}$, $CD23^-$); MZ, marginal zone B cells ($CD21^{high}$, $CD23^-$); FO, follicular B cells ($CD21^{int}$, $CD23^+$); PC, plasma cells. (E) *DUSP4* copy number alterations were analyzed using the Progenetix database. The fractions of cases affected by deletions (of 100-Mb maximum length) targeting the *DUSP4* locus are shown for the indicated lymphoma entities. A representative ABC-DLBCL array CGH profile showing a focal *DUSP4* deletion is shown in the left panel.

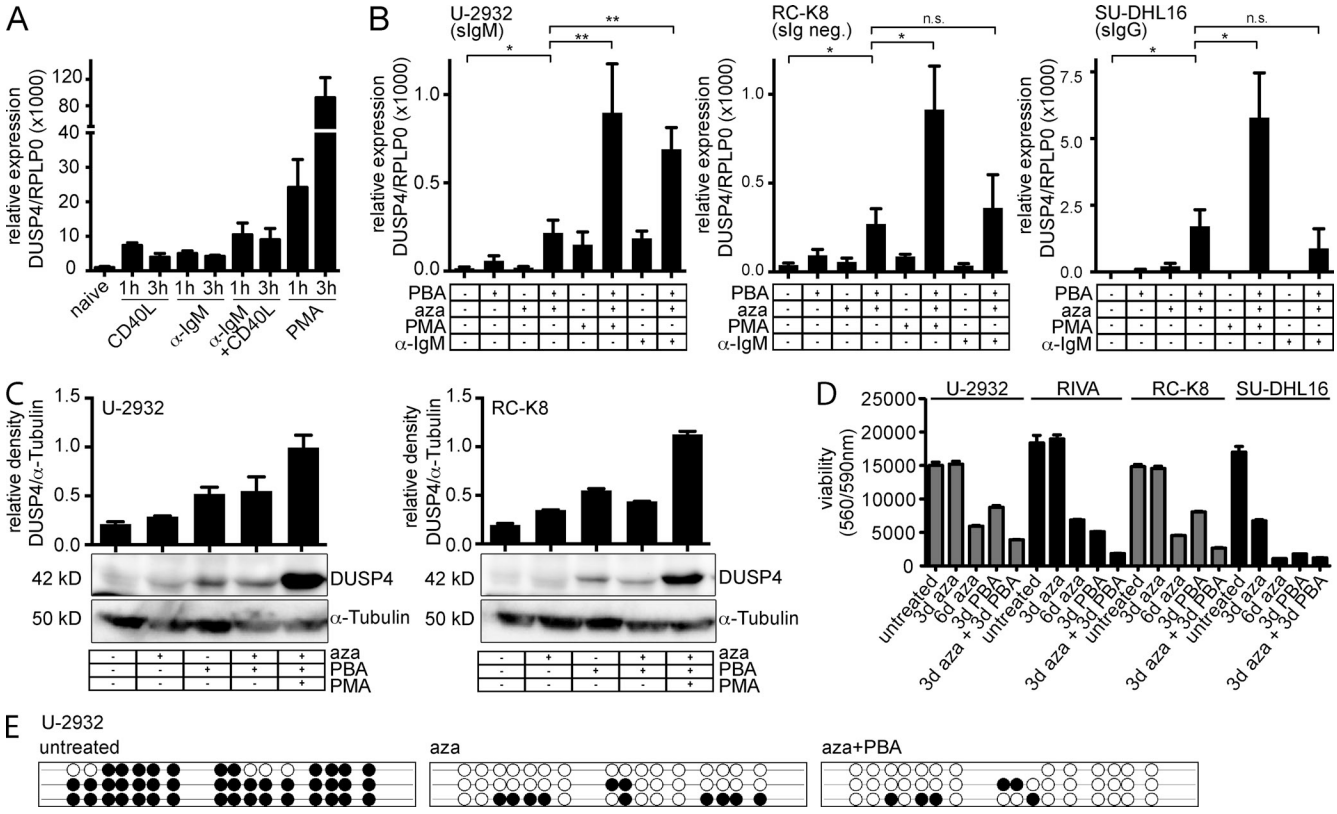

Figure 4. Combined DNA demethylation and HDAC inhibition relieves DUSP4 repression. (A) CD19+ peripheral blood B cells were stimulated with 100 nM PMA, 10 µg/ml anti-IgM, and/or 500 ng/ml CD40L for the indicated times. DUSP4 expression was assessed by qRT-PCR (normalized to RPLP0). Data represent mean + SEM of two to four blood donors. (B) DUSP4 transcript levels were measured for the three indicated DLBCL cell lines after treatment with 5 µM 5-aza-2′-deoxycytidine, 3 mM PBA, 100 nM PMA, and 10 µg/ml anti-IgM alone or in the indicated combinations. Data represent means + SEM of at least three independent experiments. *, $P < 0.05$; **, $P < 0.01$, calculated using two-tailed Student's *t* test. (C) DUSP4 protein expression was detected by immunoblotting for the two indicated DLBCL cell lines after treatment with 5 µM 5-aza-2′-deoxycytidine, 3 mM PBA, and/or 100 nM PMA; representative Western blot images are shown together with densitometric ratios of DUSP4/α-tubulin. Graphs represent mean + SEM of two independent experiments (the results represent a limited number of repeats). (D) The viability of DLBCL cell lines after treatment with 5-aza-2′-deoxycytidine and PBA, alone or in the indicated combinations, was determined by colorimetric CellTiter-Blue assay. Data are representative of two independent experiments and are shown as mean + SEM (the results represent a limited number of repeats). (E) Bisulfite sequencing of CpG island 28 was performed for untreated U-2932 cells and U-2932 cells after treatment with 5-aza-2′-deoxycytidine, either alone or in combination with PBA. Closed and open circles represent methylated and unmethylated CpGs, respectively. Three individual clones of one experiment were sequenced.

DLBCL cells only after treatment with 5-aza-2′-deoxycytidine/PBA, and only if the examined cell line actually expressed surface IgM (sIgM; Fig. 4 B). This was the case for the cell line U-2932, but not RC-K8, which is sIg negative, or SU-DHL16, which expresses sIgG (Fig. 4 B). Interestingly, 5-aza-2′-deoxycytidine/PBA treatment not only efficiently demethylated the *DUSP4* promoter and, in combination with PMA or anti-IgM, promoted DUSP4 expression, but also strongly reduced the viability of all examined DLBCL cell lines (Fig. 4, B–E). The combined results indicate that the widespread hypermethylation of the *DUSP4* promoter in DLBCL indeed results in functional DUSP4 deficiency, which can only be overcome with the appropriate stimulus if the epigenetic repression is first relieved by DNA demethylation in combination with HDAC inhibition.

Ectopic DUSP4 expression induces apoptosis in a phosphatase activity–dependent manner

To assess the effects of DUSP4 re-expression on DLBCL viability in detail, five DLBCL cell lines were electroporated with a cDNA expression construct encoding DUSP4. Ectopic expression of wild-type DUSP4 reduced cell viability and induced apoptotic cell death as assessed by CellTiter-Blue assay and annexin V staining (Fig. 5, A–C). This effect was dependent on DUSP4 enzymatic activity, as ectopic expression of a point mutant (C280S) lacking phosphatase activity (Robinson et al., 2001) did not affect the viability of DLBCL cells (Fig. 5, A–C). In line with their shared, almost universal *DUSP4* promoter methylation, GCB- and ABC-type DLBCL cell lines were equally susceptible to ectopic DUSP4 expression (Fig. 5, A–C; note that the RC-K8 subtype is controversial:

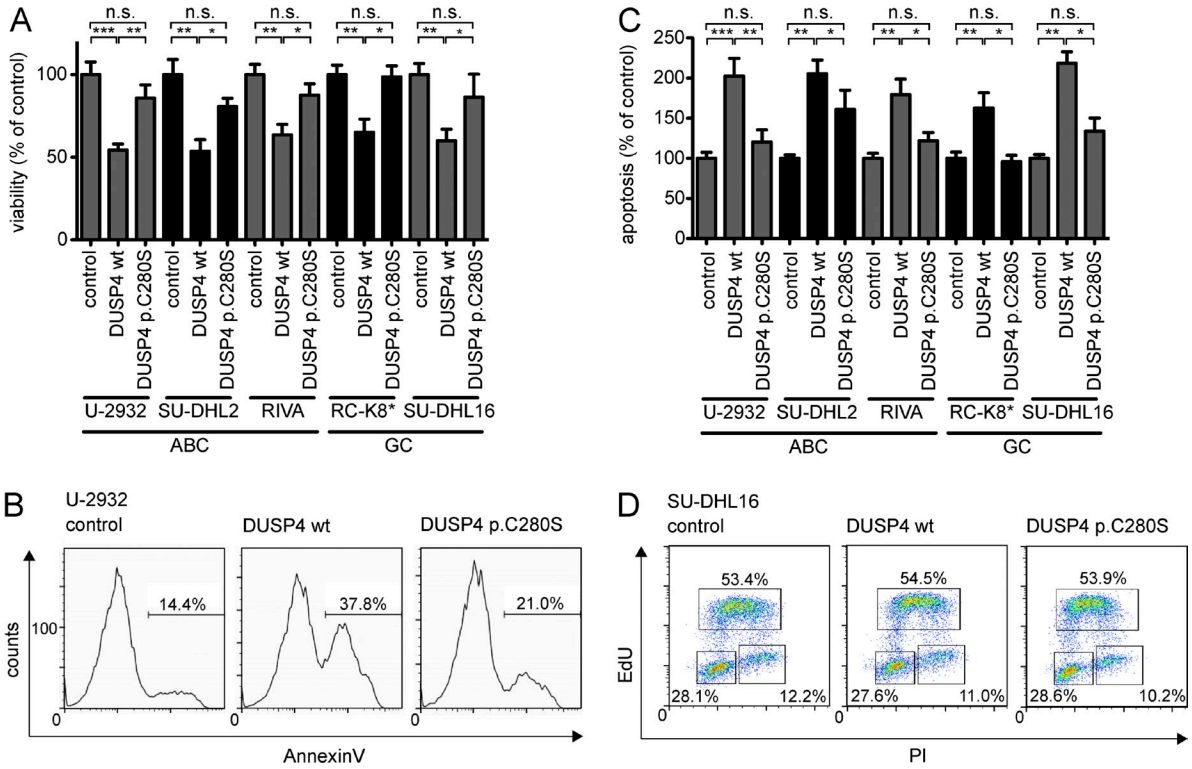

Figure 5. Ectopic DUSP4 expression decreases the viability of DLBCL cell lines by inducing apoptosis. (A) The viability of five different DLBCL cell lines was assessed 72 h after transfection with DUSP4 wt or DUSP4 p.C280S mutant constructs, relative to empty vector–transfected cells (control). Data represent means + SEM of at least three independent experiments. (B and C) Apoptosis of the same DLBCL cell lines as shown in A was assessed 72 h after transfection with DUSP4 wt or DUSP4 p.C280S mutant constructs relative to empty vector–transfected cells (control). A representative annexin V flow cytometry histogram of three independent experiments is shown in B. Data in C represent mean + SEM of at least three independent experiments per cell line. (A and C) *, $P < 0.05$; **, $P < 0.01$; ***, $P < 0.001$, calculated using two-tailed Student's *t* test. (D) Edu-PI staining of SU-DHL16 cells was performed 72 h after transfection. Representative flow cytometry dot plots of three independent experiments are shown. The numbers indicate the percentage of live cells in the G1, S, and G2-M phases of the cell cycle, respectively.

although lumped with GCB-type DLBCL here based on Lenz et al. [2007], cells may actually be of the ABC subtype [Schmitz et al., 2012]). In contrast, progression through the cell cycle was not impaired upon ectopic DUSP4 expression, as the fraction of cells in the S, G1, and G2 phases of the cell cycle did not differ in any of the cell lines, as determined by EdU incorporation assay in conjunction with propidium iodide (PI) staining (Fig. 5 D). In summary, DUSP4 has pro-apoptotic activity in DLBCL cell lines of both subtypes, and its epigenetic silencing likely provides a significant growth advantage to DLBCL cells.

JNK is the preferred and biologically relevant MAP kinase target of DUSP4 in DLBCL

DUSP4 has been described to dephosphorylate MAP kinases of the JNK, p38, and ERK families. We found JNK1/2 and two p38 family members to be expressed and constitutively phosphorylated at steady-state in 11 examined cell lines irrespective of the GCB/ABC subtype, whereas ERK1/2 is phosphorylated only in ABC-DLBCL lines (Fig. 6 A). Only JNK1 and JNK2, but not p38 or ERK1/2, were consistently dephosphorylated in ABC and GCB cell lines upon forced expression of wild-type DUSP4 (Fig. 6, B and C). ERK1/2 phosphorylation increased upon ectopic DUSP4 expression in U-2932 cells, a finding which is in line with the documented negative regulation of ERK phosphorylation by active JNK (Shen et al., 2003; Fey et al., 2012). Phosphatase-dead DUSP4 had only minor effects on JNK1/2 phosphorylation (Fig. 6, B and C). Ectopic DUSP4 expression affected the nuclear pool of JNK; immunofluorescence staining for phospho-JNK revealed a significant reduction in nuclear staining intensity in cells that had been transfected with DUSP4 relative to empty vector–transfected cells (Fig. 6, D and E). Moreover, the expression of endogenous DUSP4 induced by the IgM/CD40-mediated activation of normal human B cells also correlated with dephosphorylation of JNK (Fig. 6, F and G). The combined results suggest that JNK1/2 is the only direct MAP kinase target of DUSP4 in (normal and malignant) B cells. We next attempted to perform IHC for phosphorylated JNK on our lymphoma tissue array, which was complicated by the fact that the fixation procedures used for most spotted samples were incompatible with p-JNK detection. Nevertheless, a subset of 37 samples that allowed for both p-JNK

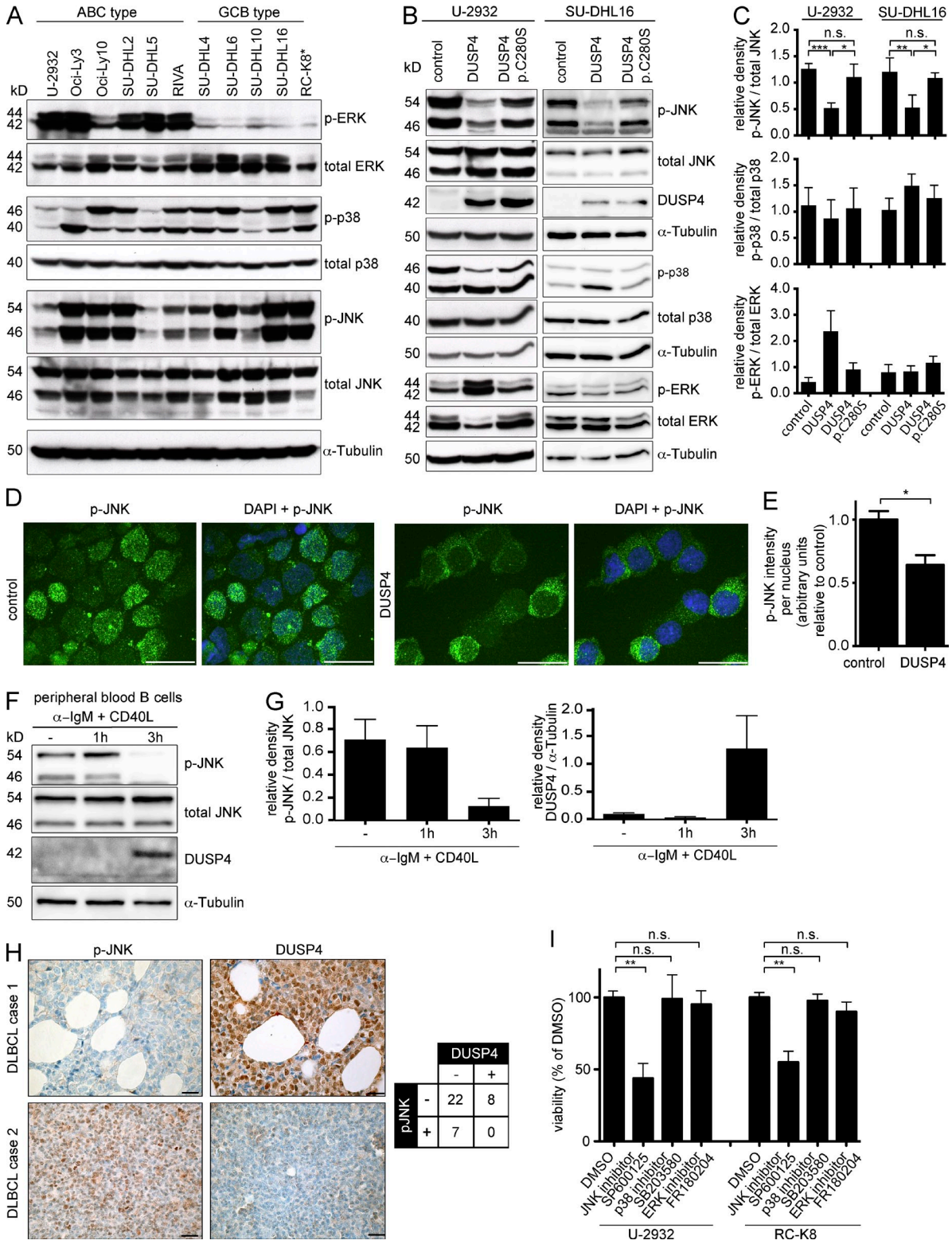

Figure 6. JNK is the preferred and biologically relevant MAP kinase target of DUSP4 in DLBCL. (A) Steady-state ERK, p38, and JNK activity was assessed in a set of six ABC- and five GCB-DLBCL cell lines by phospho-specific Western blotting. Overall protein expression of the respective kinases and of tubulin is shown for comparison. One representative of two independent experiments is shown. (B) U-2932 and SU-DHL16 cells were transfected with empty vector (control) or DUSP4 wt or DUSP4 p.C280S mutant constructs. MAP kinase activity was analyzed by phospho-specific Western blotting 72 h after transfection. p-JNK/total JNK, $n = 4$; p-p38/total 38 and p-ERK/total ERK, $n = 2$. (C) The densitometric ratio of phospho-MAPK relative to the total

and DUSP4 staining revealed the mutually exclusive expression of the two markers (Fig. 6 H), suggesting that the JNK signaling pathway is active in the absence of DUSP4.

To functionally assess which MAP kinases are not only active but also required for DLBCL survival, we next examined the effects of inhibitors blocking JNK, p38, or ERK1/2. Only a JNK inhibitor, but not inhibitors of ERK1/2 or p38, had measurable effects on U-2932 and RC-K8 viability (Fig. 6 I). The combined results suggest that DLBCL cells depend critically on active JNK signaling and that the growth advantage conferred by DUSP4 deficiency is caused by unrestricted (nuclear) JNK activity.

Pharmacological and genetic inhibition of JNK blocks DLBCL growth in vitro and in vivo

To examine the growth-inhibitory effects of JNK inhibition in more detail, we performed dose–response measurements with the ATP-competitive JNK inhibitor SP600125 in various DLBCL cell lines. Concentrations of SP600125 that strongly reduced c-JUN phosphorylation were also effective at reducing DLBCL viability and inducing apoptosis (Fig. 7, A–D). Additional inhibitors of JNK with a different mode of action, i.e., covalent irreversible binding to both JNK isoforms in the case of IN-8, and competition with scaffold protein binding in the case of BI-87G3, also exhibited dose-dependent growth inhibitory effects in all examined cell lines (Fig. 7, E and F). A genetic approach using dominant-negative constructs of JNK1 and -2 confirmed that the activity of both JNKs is critical for the survival of all examined DLBCL cell lines (Fig. 7 G).

We next investigated the effects of SP600125 in a xenograft model of DLBCL using the ABC-type cell line U-2932. SP600125 was administered every other day at 30 mg/kg body weight either starting 1 d after subcutaneous lymphoma cell implantation or once palpable tumors had formed. Both treatments significantly reduced tumor volumes as measured over time, as well as the tumor weight at the study endpoint (Fig. 7, H–J); adverse effects of the treatment on overall animal health were not observed in the time frame of the experiment. The combined results suggest that JNK inhibition reduces DLBCL viability and induces apoptosis in vitro and impairs xenograft growth in vivo.

JNK inhibition synergizes with Bruton's tyrosine kinase (BTK) inhibition to limit DLBCL growth

Ibrutinib is a novel inhibitor of BTK that has proven to be effective in ABC-DLBCL with chronic active BCR signaling in various preclinical combination treatments (Mathews Griner et al., 2014). To examine whether simultaneous JNK and BTK inhibition synergizes to kill DLBCL cells, we conducted single and combination treatments with SP600125 and ibrutinib. Ibrutinib treatment alone was insufficient to kill any of our DLBCL cell lines at concentrations up to 1 µM (Fig. 8 A). However, the addition of ibrutinib, even at very low doses of 1–10 nM, strongly boosted the efficacy of SP600125 in two ABC-DLBCL cell lines (Fig. 8, B and C). This effect was not seen in the GCB cell line SU-DHL16 (Fig. 8 D) or in an ABC-DLBCL cell line in which the BCR signaling pathway is constitutively active as the result of a *CARD11* mutation (Oci-Ly3; Fig. 8 E). In those cell lines where ibrutinib augmented the effects of JNK inhibition, the two treatments were clearly synergistic, as determined by Chalice matrix analyses and the isobologram method (Fig. 8, F and G). In summary, our data indicate that JNK inhibitors should be considered for assessment as single agents in clinical trials for both subtypes of DLBCL and might be especially promising in combination with ibrutinib in ABC-DLBCL.

Lack of DUSP4 expression is a negative prognostic factor in ABC- and GCB-DLBCL

To address whether the lack of DUSP4 expression would affect DLBCL patient survival, we analyzed three large cohorts of patients that had received standard chemotherapy consisting of cyclophosphamide, doxorubicin, vincristine, and prednisone (CHOP), with or without the addition of rituximab (R-CHOP), and had previously been subjected to microarray-based gene expression profiling (Lenz et al., 2008; Visco et al., 2012). All three cohorts were subdivided into DUSP4^{low} (lowest quartile of DUSP4 expression) and DUSP4^{high} groups (comprising the remaining three quartiles) based on their DUSP4 transcript levels, and their overall survival probability was plotted over time. In all three cohorts, high DUSP4 gene expression was associated with a superior survival probability relative to the corresponding DUSP4^{low} group, independent of the treatment regimen (Fig. 9, A–C). The largest cohort, which had received R-CHOP treatment (Visco et al., 2012),

MAPK is shown for four (JNK, top) and two (p38, middle; ERK, bottom; results represent a limited number of repeats) independent experiments. SEM is shown. (D) Immunofluorescence microscopy images of p-JNK (green) and DAPI (blue) were obtained 72 h after transfection of SU-DHL16 cells with control (empty vector) or DUSP4 wt construct. One representative picture per condition of four independent experiments is shown. (E) Mean nuclear p-JNK intensity of at least 30 nuclei per experimental condition was quantified using Cell Profiler software. Mean and SEM of four independent experiments are shown. (F) CD19$^+$ peripheral blood B cells were activated with 10 µg/ml anti-IgM and 500 ng/ml CD40L for the indicated times, followed by analysis of endogenous DUSP4 protein expression and JNK phosphorylation by Western blotting. (G) Densitometric ratios of p-JNK/total JNK (left) and DUSP4/α-tubulin (right) of two independent experiments were determined for samples as shown in F (results represent a limited number of repeats). SEM is shown. (H) 37 clinical cases of DLBCL were stained for DUSP4 protein expression and p-JNK by IHC. Representative micrograph images of two DLBCL cases are shown in the left panel. The relationship of DUSP4 and p-JNK expression is shown in a contingency table (right). The p-value was calculated by χ^2 test ($P = 0.152$, $n = 37$). Bars: (D) 25 µm; (H) 50 µm. (I) The viability of U-2932 and RC-K8 cells was determined by CellTiter-Blue assay after 72 h of treatment with 50 µM SP600125 (JNK inhibitor), SB203580 (p38 inhibitor), or FR180204 (ERK inhibitor) relative to DMSO-treated cells. Means + SEM of three independent experiments are shown. (C, E, and I) *, $P < 0.05$; **, $P < 0.01$; ***, $P < 0.001$, calculated by two-tailed Student's *t* test.

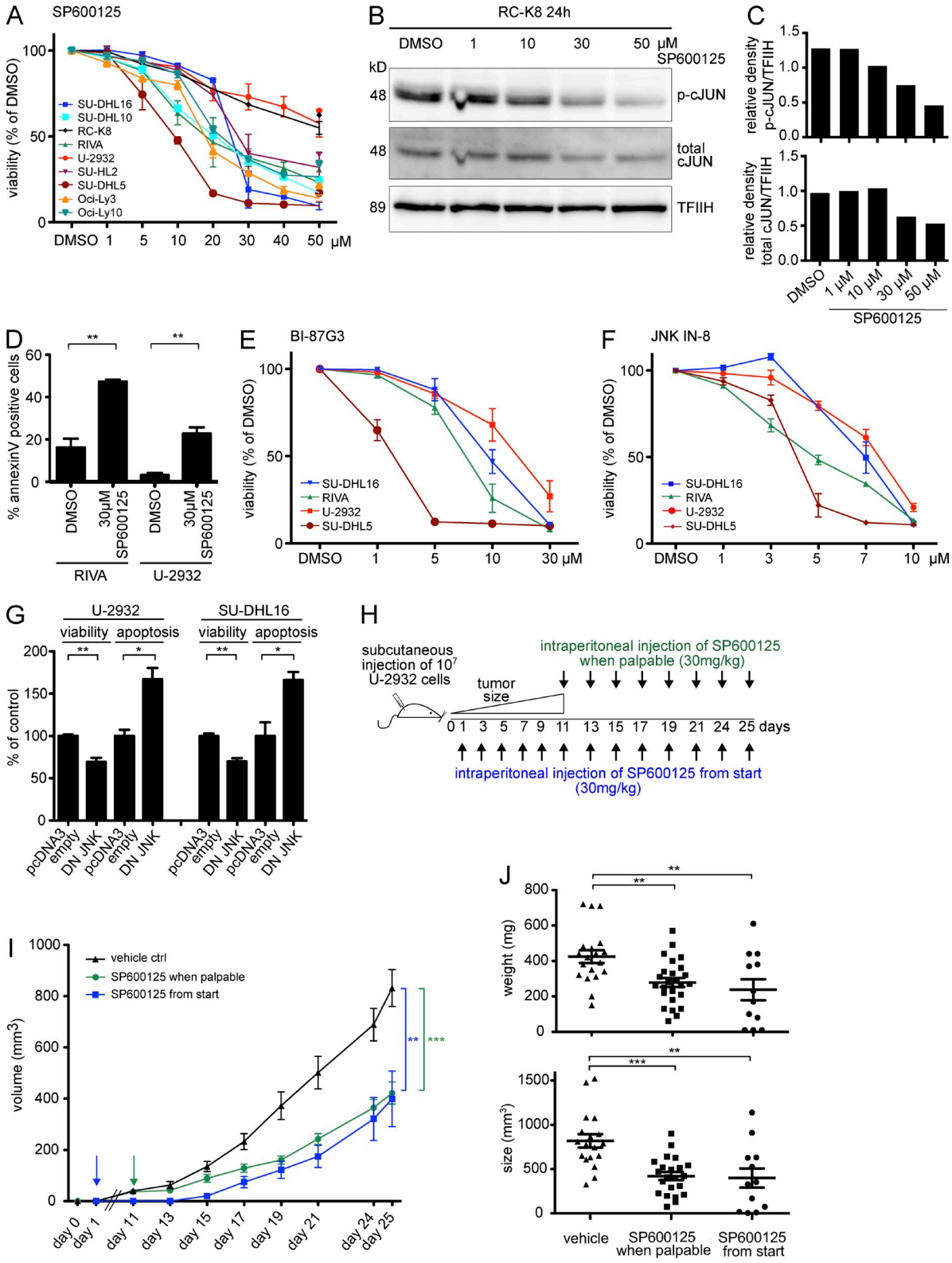

Figure 7. Pharmacological and genetic inhibition of JNK blocks DLBCL growth in vitro and in vivo. (A) The viability of the DLBCL cell lines indicated was determined by CellTiter-Blue assay after 72 h of treatment with increasing concentrations of the JNK inhibitor SP600125 relative to DMSO-treated cells. Means + SEM for two to four independent experiments per cell line are shown. (B) A Western blot analysis of phosphorylated c-JUN (representative of three independent experiments), total c-JUN, and TFIIH expression (loading control) after 24 h of treatment with the indicated concentrations of SP600125 is shown. (C) Densitometric ratios of phospho–c-JUN/TFIIH and total c-JUN/TFIIH were calculated for the samples shown in B. (D) Apoptosis of RIVA and U-2932

was further stratified into ABC- and GCB-type DLBCL patients based on overall gene expression signatures and subjected to subtype-specific survival analysis. As reported previously (Visco et al., 2012), both subtypes differed strongly in terms of their overall survival probability, with GCB-DLBCL patients surviving longer than their ABC-DLBCL counterparts (compare Fig. 9, D and E). In each subtype, high DUSP4 expression was associated with significantly superior survival (Fig. 9, D and E), indicating that the expression of DUSP4 serves as a positive prognostic factor for survival prediction in DLBCL, irrespective of subtype and therapeutic regimen. The results confirm and extend our experimental data and demonstrate that DUSP4 is not only a likely tumor suppressor in DLBCL, but also has prognostic value for survival prediction independent of subtype.

DISCUSSION

In this study, we have performed a genome-wide DNA methylome analysis of DLBCL cell lines and primary patient material followed by an unbiased functional assessment of the tumor-suppressive properties of the 30 top epigenetically silenced candidates. Several unexpected observations were made in the course of our methylome analyses. First, although several thousand aberrantly methylated genes were identified in our gastric set of lymphoma cases, the methylation patterns were very similar in low-grade MZL of MALT and high-grade gastric DLBCL. This was particularly striking given the vast differences in the aggressiveness and clinical prognosis of the two lymphoma entities. Three pairs of consecutively isolated low- and high-grade samples from the same patient confirmed this general trend; no obvious differences were detected within the pairs. In fact, two of the three even clustered together on very short branches of the dendrogram tree, documenting their highly similar DNA methylation patterns. Aberrant promoter hypermethylation thus appears to constitute an early rather than late event in gastric lymphomagenesis. A detailed comparison of the promoter-associated CpG island methylation profiles of our own gastric lymphoma set with those of nodal DLBCL cases further revealed the striking similarity of nodal and extranodal cases with respect to their methylomes. With the exception of a handful of cases in every sample set that did not share the general methylation patterns of all others and instead clustered with the unmethylated controls, all nodal and gastric cases exhibited a highly consistent methylation profile. This observation suggests that both types share a common pathogenetic mechanism irrespective of the affected site and the underlying cause of the disease, which is likely infectious in the gastric form (Isaacson and Du, 2004) and largely unknown in the nodal form.

The methylation of the promoter regions of most of the genes that we identified by array could be verified using bisulfite sequencing; false-positive hits were rare. However, not all of the hypermethylated genes could be reactivated by global pharmacological demethylation, indicating that these are not expressed by DLBCL cells, at least under in vitro culture conditions. Of the 30 hypermethylated genes that were reactivated upon DNA demethylation and therefore selected for individual functional assessment, only eight were found to affect cell viability. The dysregulation of one of the eight, the dual-specificity phosphatase DUSP4, proved to be particularly widespread and biologically meaningful in the extranodal as well as nodal forms of the disease, warranting further in depth analyses of the affected signaling pathways. The biology of DUSP4, which dephosphorylates both phosphoserine/threonine and phospho-tyrosine residues on its MAP kinase substrates, is poorly understood in the context of cancer. The silencing of DUSP4 by promoter hypermethylation was reported in the past for certain forms of secondary glioblastomas and anaplastic astrocytomas (Waha et al., 2010), as well as basal-like breast cancer (BLBC), where low DUSP4 transcript levels after neoadjuvant chemotherapy have been linked to MEK–ERK pathway activation and chemotherapy resistance (Balko et al., 2012). Follow-up analyses have attributed the effects of DUSP4 loss in BLBC to the maintenance of a cancer stem cell population, which is dependent on active JNK and ERK signaling and MAP kinase–dependent IL-6 as well as IL-8 production (Balko et al., 2013). DUSP4 promoter methylation of the CpG island 344 was also recently reported as part of a broader methylation signature for several types of lymphoma, including Burkitt lymphoma, FL, and ABC-DLBCL (Bethge et al., 2014). Although limited by the rather small number of analyzed cases, the study found a trend toward higher methylation frequencies in ABC- compared with GCB-DLBCL (Bethge et al., 2014). We report here that methylation of the CpG island 28 in the *DUSP4* promoter region serves as a reliable indicator of the lack of DUSP4 expression in various subtypes, i.e., nodal and extranodal, ABC and GCB, of DLBCL: the region is methylated in

cells was assessed after 72 h of treatment with 30 µM SP600125, as measured by annexin V staining. Mean and SEM of three independent experiments are shown. (E and F) The viability of DLBCL cell lines was assessed after 72 h of treatment with the indicated concentrations of the JNK inhibitors BI-87G3 and JNK-IN-8. Mean + SEM of at least three independent experiments is shown. (G) The cell viability and apoptosis of the two indicated DLBCL cell lines was determined by CellTiter-Blue assay and annexin V staining 72 h after transfection with dominant-negative JNK constructs (1.5 µg pCDNA3-JNK1a1(apf) + 1.5 µg pcDNA3-JNK2a2(apf)) and are presented as percentage values relative to empty vector–transfected cells. Mean + SEM of three independent experiments are shown. (D and G) *, $P < 0.05$; **, $P < 0.01$, calculated using two-tailed Student's *t* test. (H–J) NOD/SCID/IL2R$\gamma^{-/-}$ mice were subcutaneously inoculated in both flanks with 10^7 U-2932 cells. Mice were treated every other day with 30 mg/kg SP600125 i.p. starting on day 1 after transplantation (blue) or when tumors were palpable (day 11, green) as shown in the diagram in H. Tumor growth in I was measured as a function of tumor volume, which is represented as means ± SEM. Vehicle control, $n = 9$ mice (18 individual tumors); treatment from start, $n = 6$ mice (12 tumors); treatment when palpable, $n = 11$ mice (22 tumors). The top and bottom panels in J show tumor weights and tumor volumes at the study endpoint. **, $P < 0.01$; ***, $P < 0.001$, one-way analysis of variance with Bonferroni's post-test. Pooled data from two experiments are shown in I and J.

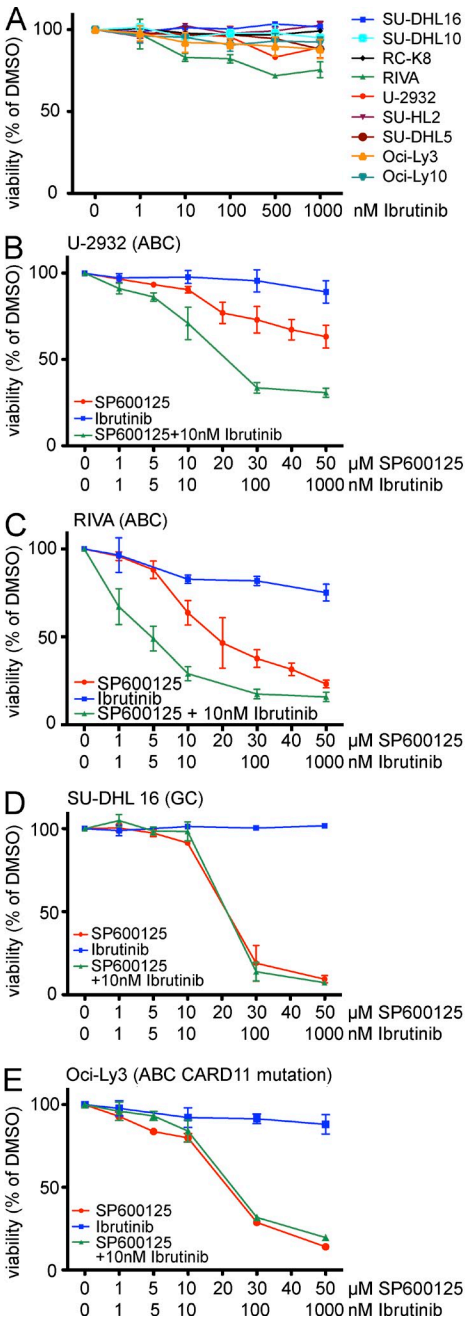

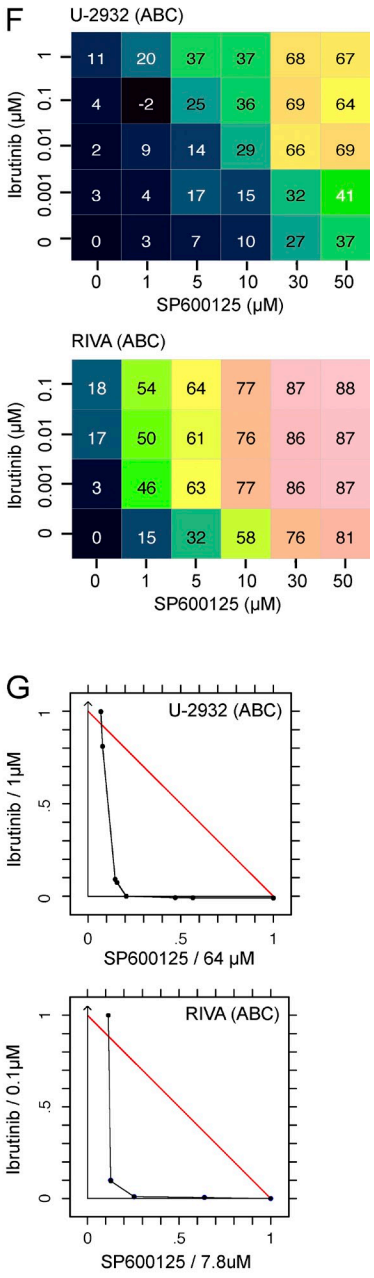

Figure 8. The JNK inhibitor SP600125 synergizes with ibrutinib in killing ABC-DLBCL cell lines. (A) The viability of DLBCL cell lines was determined by CellTiter-Blue assay after 72 h of treatment with the indicated concentrations of the BTK inhibitor ibrutinib and calculated relative to DMSO-treated cells. Means ± SEM for two to four independent experiments per cell line are shown. (B–G) The viability of the indicated DLBCL cell lines was assessed after 72 h of treatment with increasing concentrations of the JNK inhibitor SP600125 and the BTK inhibitor ibrutinib, either alone or in combination, relative to DMSO-treated cells. In F, Chalice Analyzer inhibition matrices are shown for combination responses to SP600125 and ibrutinib of the indicated cell lines. In G, isobolograms of viability data demonstrating drug synergy are shown for the indicated cell lines. The results presented in G were compiled from B, C, and F. In B, C, F, and G, data from at least three and up to four independent experiments are shown; in D and E, data from two independent experiments (results represent a limited number of repeats) are shown. Results in A–E are presented as means ± SEM.

all cell lines lacking DUSP4 expression, and there is a clear inverse correlation of DUSP4 expression and methylation status in all analyzed clinical cases. The opposite is seen in clinical cases of CLL, which largely exhibit unmethylated *DUSP4* promoters and express high levels of the protein. Exposure to 5-aza-2′-deoxycytidine, especially in combination with HDAC inhibition, clearly reduces *DUSP4* CpG island 28 methylation and promotes DUSP4 re-expression. The dependence of the phenotype on HDAC inhibition is explained by our preliminary data showing that active histone marks (such as H3K9ac and H4ac) are lost and repressive histone marks are enriched on CpG island 28 of the DUSP4 promoter in DLBCL cells (unpublished data).

In accordance with the aberrant epigenetic silencing of the *DUSP4* genomic locus in DLBCL, we found that DUSP4 expression levels can be used for survival prognostication. The lack of DUSP4 expression was a clear negative prognostic factor in multiple large cohorts of DLBCL, irrespective of the applied treatment regimen (CHOP vs. R-CHOP) and subtype of DLBCL analyzed. The combined results of the regulation of DUSP4 expression by DNA methylation and histone modification, and its value as a survival factor, together imply

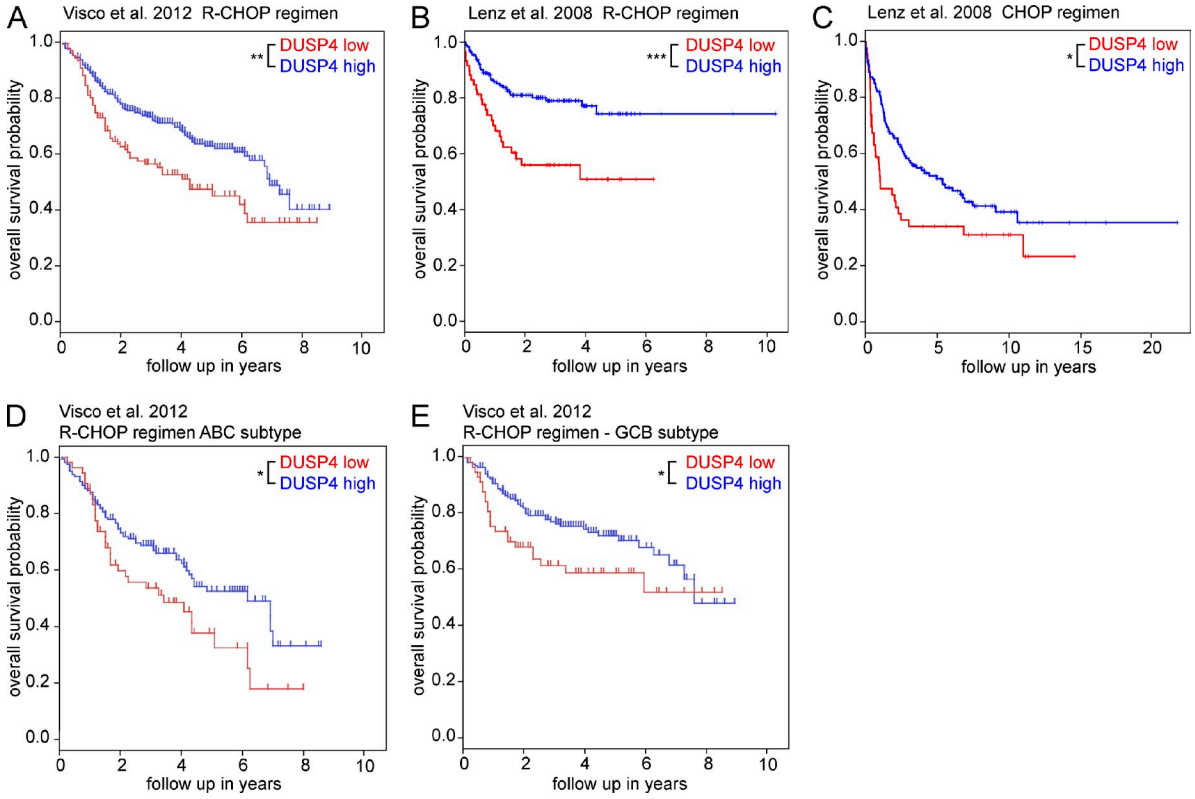

Figure 9. The level of DUSP4 expression correlates with overall survival of DLBCL patients. (A–C) Kaplan–Meier curves displaying overall survival of three DLBCL patient cohorts (GEO accession nos. GSE31312 and GSE10846) treated with R-CHOP (rituximab, cyclophosphamide, hydroxydaunorubicin, vincristine, and prednisone; A and B) or CHOP (cyclophosphamide, hydroxydaunorubicin, vincristine, and prednisone; C) as a function of DUSP4 mRNA expression are shown. (D and E) Kaplan–Meier curves displaying overall survival probability based on DUSP4 mRNA expression in ABC (D) and GCB (E) subsets of DLBCL patients are shown. (A–E) All cohorts were subdivided based on low (first quartile) and high (second to fourth quartile) DUSP4 expression. The log-rank test was used for statistical analysis: *, $P < 0.05$; **, $P < 0.01$; ***, $P < 0.001$. Visco et al. (2012), $n = 470$; ABC subtype, $n = 226$; GCB subtype, $n = 242$; Lenz et al. (2008) R-CHOP, $n = 233$; Lenz et al. (2008) CHOP, $n = 181$. The Lenz et al. (2008) dataset was analyzed using R software, and the Visco et al. (2012) data were analyzed using the R2 microarray analysis and visualization platform (http://r2.amc.nl).

that DNA methyltransferase inhibitors and HDAC inhibitors should be considered for the treatment of DLBCL patients with DUSP4-negative tumors, especially given that compounds belonging to both classes of drugs are approved and/or in clinical development for the treatment of other hematological malignancies (Dhanak and Jackson, 2014).

In line with a putative tumor suppressor activity of DUSP4 in DLBCL, we found that ectopic expression of the wild-type protein, but not the C280S point mutant lacking phosphatase activity, induced apoptosis in all examined DLBCL cell lines. Apoptosis occurred as a direct result of DUSP4 expression rather than as a secondary consequence of cell cycle arrest and was mediated by the DUSP4-dependent inactivation of JNK signaling. In accordance with these findings, the pharmacological or dominant-negative inhibition of the two JNKs, but not of ERK or of p38, phenocopied the cytotoxicity of forced DUSP4 re-expression, suggesting that the JNK signaling pathway is more critical than the other two to the survival of DLBCL cell lines. Our data thus differ from the proposed mechanism of DUSP4 silencing in BLBC, where the MEK–ERK pathway has predominantly been implicated in cancer stem cell maintenance and therapy resistance (Balko et al., 2013). JNK inhibition not only promoted apoptosis of DLBCL cell lines upon in vitro treatment, but also effectively delayed tumor growth and reduced tumor burden in a xenograft model of DLBCL. The effects of JNK inhibition were not only preventive, but also therapeutic in our hands, as established tumors also grew more slowly under systemic JNK inhibitor treatment. JNK inhibition represents a largely untested strategy in hematopoietic malignancies, and only sporadic studies exist in the literature. In vitro studies suggest that JNK signaling may be active and may contribute to tumor cell proliferation in certain cases of MCL and classical Hodgkin lymphoma (Wang et al., 2009; Leventaki et al., 2014); JNK signaling is also known to be active in TNF-secreting acute myelogenous leukemia cells (Volk et al., 2014). Consequently, inhibition of JNK signaling impaired the growth of Hodgkin and Reed-Sternberg cells and of MCL cell lines and acute myelogenous leukemia cells in vitro, either as single treatment or in combination (Wang et al., 2009; Boukhiar et al., 2013; Leventaki et al., 2014;Volk et al., 2014). In vivo efficacy has further been shown for JNK inhibition in xenografts of immature B cell

lymphomas, glioblastomas, and colorectal cancer, also without evidence of adverse effects (Jemaà et al., 2012; Matsuda et al., 2012).

To test whether our approach of JNK inhibition may be combined with existing therapeutic strategies to achieve synthetic lethality, we conducted coinhibition experiments with ibrutinib, which is approved and marketed for high-risk CLL and refractory MCL and is currently in phase 2 trials for ABC-DLBCL. Ibrutinib clearly synergized with JNK inhibition to reduce the viability and induce apoptosis of certain DLBCL cell lines but not others. Interestingly, only ABC-DLBCL with an unmutated BCR signaling pathway, but not GCB-DLBCL or a *CARD11* mutant ABC-DLBCL cell line, responded to the SP600125/ibrutinib combination. This result is in line with a critical role for chronic active BCR signaling in ABC, but not GCB-DLBCL survival (Davis et al., 2010), and the general observation that ibrutinib efficacy is limited to ABC-DLBCL with an unmutated BCR signaling pathway leading to constitutive oncogenic IκB kinase and NF-κB activity (Ceribelli et al., 2014).

In summary, by applying an approach from bedside to bench and back to preclinical models, we have identified a novel pathogenetic mechanism in DLBCL that relies on the epigenetic silencing of the *DUSP4* promoter, a widespread phenomenon in both extranodal and nodal cases. DUSP4 deficiency gives rise to a constitutively active JNK signaling pathway, which can in turn be targeted pharmacologically to reduce tumor cell survival and prevent tumor progression in vitro and in vivo. Our results provide a mechanistic basis for the clinical development of JNK inhibitors for the treatment of DLBCL, particularly in a synthetically lethal combination with novel therapies targeting chronic active BCR signaling.

MATERIALS AND METHODS

Patient samples and cell culture. For whole-genome methylation analysis and bisulfite sequencing, archived patient material of gastric low-grade MZL of MALT, nodal, extranodal, and transformed DLBCL, CLL, and reactive tonsils was drawn from the surgical pathology files of the Institute of Pathology at the Cantonal Hospital St. Gallen and from the files of the Institute of Pathology, University Hospital Basel. Diagnosis was established according to the classification system of the World Health Organization (WHO) on formalin-fixed, paraffin-embedded (FFPE) tissue. All data were blinded to guarantee patient protection. All procedures were in agreement with the guidelines for use of human material in research issued by the Ethics Committee of the Cantonal Hospital St. Gallen and the Ethical Committee of North-Western Switzerland. The DLBCL cell lines used were SU-DHL4, SU-DHL6, SU-DHL10, SU-DHL16, and RC-K8 of GCB-DLBCL subtype and U-2932, Oci-Ly3, Oci-Ly10, SU-DHL2, SU-DHL5, and RIVA of ABC-DLBCL, as well as SU-DHL7 (unclassified). Cell lines were maintained at 37°C, 5% CO_2 in a humidified atmosphere in RPMI or IMDM (RIVA and Oci-Ly10) supplemented with 10% (Oci-Ly10, RIVA, SU-DHL2, and SU-DHL5) or 20% heat-inactivated FBS and antibiotics. CD19-positive B cells were isolated from buffy coats of healthy volunteer blood donors obtained from the blood donation center Zürich (ZHBSD) by immunomagnetic sorting and cultured in RPMI, 10% FCS, 2 mM L-glutamine, 50 µM β-mercaptoethanol, 2 ng/ml hIL-4 (eBioscience), and antibiotics.

Transient transfection of DLBCL cell lines, pharmacological treatments and viability, cell cycle, and apoptosis assays. For the purpose of ectopic gene expression, 10^6 DLBCL cells were nucleoporated with 3 µg plasmid DNA using the Amaxa Nucleofector II device (Lonza). Cells were harvested 72 h after transfection for protein extraction or subjected to functional analysis. For drug treatments, cells were seeded at a density of 0.4×10^6/ml with the respective drug concentration and analyzed for cell viability or apoptosis 72 h later. For viability assays, 50 µl of cell suspension was transferred into 96-well plates containing 50 µl fresh medium in triplicates 72 h after treatment/electroporation. 20 µl CellTiter-Blue reagent (Promega) was added, and plates were incubated for 4 h at 37°C, 5% CO_2 in a humidified atmosphere. Viability was subsequently assessed by measuring fluorescence at 560Ex/590Em using a SpectraMax M5 microplate reader (Molecular Devices). For drug combination experiments, percent viability/inhibition was calculated in Excel (Microsoft) relative to DMSO-treated wells. Formatted data were analyzed by Chalice Analyzer (Horizon) to generate inhibition matrices and to assess the presence and extent of synergism by isobologram analysis. The quantification of apoptosis by an Annexin V detection kit (BD) was performed according to the manufacturer's instructions. Flow cytometry was performed on a Cyan ADP 9 instrument (Beckman Coulter) and analyzed using FlowJo software. For cell cycle analysis, the Click-IT EdU cytometry assay kit (Invitrogen) was used in combination with PI staining. Cells were incubated with 10 µM EdU for 90 min, followed by fixation, permeabilization, and intracellular staining according to the manufacturer's instructions. 100 µg/ml RNase A and 20 µg/ml PI were added for 30 min before flow cytometric analysis.

Animal experimentation. U-2932 cells were injected subcutaneously into both flanks of 6–8-wk-old NOD/SCID/IL2Rγ$^{-/-}$ mice (The Jackson Laboratory). SP600125 was dissolved in 10% DMSO, 2% Tween 80, and 2% PEG600 in PBS. 1 d after tumor cell injection or when palpable tumors had formed (~40 mm^3), mice were i.p. injected with 30 mg/kg SP600125 or vehicle every other day. Tumor volumes were measured using the formula $(a^2 \times b)/2$, where a is the shorter and b the longer tumor dimension. All animal experiments were reviewed and approved by the Zürich Cantonal Veterinary Office (licenses 147/2011 and 224/2014).

Global methylation profiling and RNA sequencing. Genomic DNA was isolated from archived FFPE biopsies of seven low-grade MZLs of MALT, nine high-grade gastric DLBCL cases, and four reactive tonsil samples using the RecoverAll Total Nucleic Acid Isolation kit for FFPE material (Life Technologies). In addition, genomic DNA was extracted from healthy peripheral blood B cells of two donors and six nodal DLBCL cell lines using the NucleoSpin tissue kit (MACHEREY-NAGEL). Global methylation profiling of these samples was performed on 450K Infinium arrays (Illumina) at the USC Epigenome Center core facility, Los Angeles. For RNA sequencing, CD19-positive peripheral blood B cells were activated with 10 µg/ml anti-IgM (SouthernBiotech) and 500 ng/ml CD40L (eBioscience) for 44 h. ABC-DLBCL cell lines (U-2932 and Oci-Ly10) were treated with 5 µM 5-aza-2′-deoxycytidine (Sigma-Aldrich) for 3 d, followed by 16 h with 3 mM PBA (Sigma-Aldrich). RNA from the B cells and cell lines was isolated using the miRNeasy Mini kit (QIAGEN). RNA quality was assessed by Bioanalyzer 2100 followed by library preparation using the TruSeq RNA Sample Prep kit v2 (Illumina). Sequencing was subsequently performed on the HiSeq 2000 instrument (Illumina). All data are accessible through Array Express: RNA-seq, E-MTAB-2925; 450K methylation data, E-MTAB-2926. Methylation data for nodal DLBCL cases and additional CD19$^+$ B cells (controls) were retrieved from GEO accession nos. GSE37365 and GSE35069 and the Cancer Genome Atlas.

Processing of DNA methylation and RNA sequencing data. R version 3.0.2 and minfi version 1.8.9 were used to process the HumanMethylation450 array data. Raw 450K array data were normalized by applying the preprocess Illumina function using bg.correct = TRUE and normalize = "controls." Probes were filtered according to suggestions from Price et al. (2013), eliminating probes that map to multiple locations in the human genome or overlap known polymorphic sites in their target CpG. After filtering, we focused only on probes in regions near annotated CpG islands, again

using the reannotated tables from Price et al. (2013) to associate CpG islands with transcriptional units. We then calculated summaries at the CpG island level by taking the median of β values for the probes in those regions (transcription start sites, first exons, 5′UTR, and regulatory elements) for each sample. CpG islands were filtered to only those that had a range in β values (consensus methylation estimate) over all samples of at least 0.25. Hierarchical clustering was conducted using the fastcluster version 1.1.13 using 1-Spearman correlation distance metric and "complete" linkage. RNA-seq reads were quality-checked with fastqc, which computes various quality metrics for the raw reads. RNA-seq FASTQ files were mapped to the hg19 reference human genome using tophat2 (Kim et al., 2013), and reads were counted according to Entrez Gene annotation using the summarizeOverlaps function in the GenomicAlignments Bioconductor package (Lawrence et al., 2013). Statistical analysis of differential expression was conducted with the edgeR package (Anders et al., 2013) using a design matrix that gives the pairing Oci-Ly10 treated with 5′-aza/PBA and untreated; U2932 treated with 5′-aza/PBA and untreated.

Cell sorting and immunomagnetic cell separation. $CD19^+$ B cells were isolated from peripheral blood of healthy blood donors using the MACS human CD19 microbeads (Miltenyi Biotec). For isolation of $CD138^+$ plasma cells from mouse bone marrow, the CD138 plasma cell isolation kit (Miltenyi Biotec) was used according to the manufacturer's protocol. For isolation of T cells and B cell subsets from mouse spleens, single cell suspensions were prepared, incubated with Fc-block (Miltenyi Biotec), and stained with B220-PB (BioLegend), CD21/35-APC (BD), CD23-PE-Cy7 (BioLegend), and CD3-PE (eBioscience). Cell sorting was performed at the University of Zürich Flow Cytometer Core Facility on an Aria III instrument (BD).

Kinase inhibitors, plasmid constructs, and site-directed mutagenesis. The JNK inhibitors SP600125 and JNK-IN-8 and the BTK inhibitor Ibrutinib were obtained from Selleckchem. The JNK inhibitor BI-87G3 as well as inhibitors of p38 (SB203580) and ERK1/2 (FR180204) were purchased from Sigma-Aldrich. Overexpression constructs used in the functional screen were obtained from Origene in the pCMV6 vector or from Biocat in the pTCN or pCMV-Sport6 backbones. Plasmids expressing a dominant-negative form of JNK (Gupta et al., 1996) were obtained from R.J. Davis (University of Massachusetts Medical School, Worcester, MA) through Addgene (plasmid number 13761, 13846). A phosphatase-inactive mutant of DUSP4, in which cysteine 280 in the wild-type DUSP4 sequence (pTCN-BC002671, Origene) is replaced by a serine, was generated using GENEART site-directed mutagenesis (Invitrogen) as described previously (Robinson et al., 2001).

Bisulfite sequencing. Genomic DNA was isolated from FFPE tissue or fresh material using the RecoverAll total RNA Isolation kit (Life Technologies) or the NucleoSpin tissue kit, respectively. 1 µg gDNA was converted with sodium bisulfite as previously reported (Frommer et al., 1992) using the EpiTect bisulfite kit (QIAGEN). Bisulfite-converted DNA was amplified with primers specific for the CpG island 28 in the DUSP4 promoter (fwd, 5′-TGGATTTGATTGTTATTTATTGGTTA-3′; rev, 5′-CAAAACATTTCTAAAAAAAACCTCTC-3′) and subcloned into the pGEM-T vector. The methylation status was subsequently assessed by sequencing the amplified *DUSP4* promoter region and analyzed using the quantification tool for methylation analysis (QUMA; Kumaki et al., 2008).

Real-time PCR. RNA was extracted using the NucleoSpin RNA II kit (MACHEREY-NAGEL) or the RNeasy micro kit (QIAGEN) in the case of FACS-sorted samples. 1 µg total RNA was reverse transcribed using SuperScriptIII reverse transcription (Invitrogen). For quantitative RT-PCR (qRT-PCR), LightCycler 480 Cyber Green Master I (Roche) was used followed by analysis on a LightCycler 480 instrument. Samples were measured in duplicates. For all primer pairs, the efficiency was calculated by performing dilution series experiments. Target mRNA abundance was subsequently calculated relative to human RPLP0 or mouse Gapdh. The primers used were the following: human DUSP4 fwd, 5′-TGCATCCCAGTGGAAGATAA-3′; and rev, 5′-GCAGTCCTTCACGGCATC-3′; human RPLP0 fwd, 5′-CCAGCTCTGGAGAAACTGCTG-3′; and rev, 5′-CAGCAGCTGGCACCTTATTGG-3′; mouse Dusp4 fwd, 5′-ATCCCCGTCGAAGACAACC-3′; and rev, 5′-CGCCCTCGACAGTCCTTTAC-3′; and mouse Gapdh fwd, 5′-GACATTGTTGCCATCAACGACC-3′; and rev, 5′-CCCGTTGATGACCAGCTTCC-3′.

Western blotting, IHC, and immunofluorescence microscopy. Protein extracts were made in RIPA buffer (50 mM Tris-HCl, pH 8.0, 150 mM sodium chloride, 1% NP-40, 0.5% sodium deoxycholate, and 0.1% SDS) supplemented with 2 mM sodium orthovanadate, 15 mM sodium pyrophosphate, 10 mM sodium fluoride, and 1× complete protease inhibitor cocktail (Roche). Protein concentrations were determined using BCA assay (Thermo Fisher Scientific), and equal amounts were separated by SDS-PAGE followed by transfer onto nitrocellulose membranes. Membranes were probed with antibodies against DUSP4 (D9A5), phospho-p38 Thr180/Tyr182 (D3F9), total p38 (D13E1), phospho-ERK1/2 Thr202/Tyr204 (D13.14.4E), total ERK (137F5), phospho-SAPK/JNK Thr183/Tyr185 (81E11), and total SAPK/JNK (56G8; all from Cell Signaling Technology), as well as phospho–c-JUN Ser63 (Y172; EMD Millipore), total c-JUN (5B1; Abcam), tubulin (DM1A; Sigma-Aldrich), and TFIIH p89 (s-19; Santa Cruz Biotechnology, Inc.). If applicable, blots were first incubated with phospho-specific antibodies and then stripped in 10 ml of 10% SDS, 6.25 ml of 0.5 M Tris-HCl, pH 6.8, 33.75 ml H_2O, and 400 µl β-mercaptoethanol for 30 min at 50°C, followed by incubation with the respective phosphorylation-independent antibodies. Quantification was performed using ImageJ 1.48v software (National Institutes of Health).

Tissue microarrays with 170 primary nodal DLBCLs, 87 extranodal DLBCLs (stomach and testis), 9 DLBCLs transformed from low-grade lymphomas, 54 MZLs of MALT, 48 FLs, and 20 small lymphocytic B cell lymphomas (SLLs)/CLL, as well as 9 MCLs were constructed as described previously (Muenst et al., 2010). For the cases studied on conventional slides (i.e., 12 nodal DLBCLs, 5 extranodal DLBCLs, 2 transformed DLBCLs, 3 CLL/SLLs, and 2 MZLs, as well as 3 normal tonsils), blotting-based quantitative protein expression data were available, thus allowing validation of the immunohistochemical analysis. The cases were classified as GCB or non-GCB–like (ABC) DLBCL applying the Tally algorithm (Meyer et al., 2011). DUSP4 staining was established by application of the primary antibody sc-10797 from Santa Cruz Biotechnology, Inc. (best working dilution 1:20) to tonsils, breast, and colon cancer, whereas pJNK staining was established by application of the primary antibody 4668 from Cell Signaling Technology (best working dilution 1:50). IHC was performed on an automated immunostainer (Benchmark; Ventana/Roche). Antigen retrieval was achieved by mild cell conditioning (CC1 from Ventana/Roche) treatment for 16 min in the case of DUSP4 and for 92 min in the case of pJNK. Primary antibody incubation was performed for 32 min in the case of DUSP4 and for 120 min in the case of pJNK before visualization (chromogen ultraview universal diaminobenzidine from Ventana/Roche). Finally, slides were counterstained with hematoxylin and bluing reagent from Ventana/Roche. The proportion of positively staining tumor cells (steps: 0, 1, 5, 10, 15, and 20%, followed by 10% steps) as well as the subcellular localization (membranous, cytoplasmic, and nuclear) were all taken into consideration. pJNK showed exclusive nuclear staining, whereas DUSP4 intensively stained nuclei but also showed some weak cytoplasmic background staining. For both DUSP4 and pJNK, only nuclear signals were considered. 30% cut-off scores were applied. For phospho-JNK–specific immunofluorescence microscopy, SU-DHL16 cells were electroporated as described above, cytospun onto glass slides, fixed for 15 min in 4% formaldehyde in PBS, blocked for 60 min at room temperature in PBS, 1% goat serum, and 0.3% Triton X-100, and stained overnight at 4°C with anti–p-JNK (4668 from Cell Signaling Technology; 1:400) in PBS, 1% BSA, and 0.3% Triton X-100, followed by detection with a Alexa Fluor 488–coupled goat anti–rabbit secondary antibody (Life Technologies; 1:400; 1 h at room temperature). Nuclei were counterstained with DAPI and covered with fluorescent mounting medium (S3023; Dako). Cells were imaged on a DM RB microscope (Leica) equipped with a DFC 360 FX camera (Leica). Images were taken with an HCX PLAPO 63×/1.4-0.6 oil immersion objective

(Leica) using the Application Suite 3.3.0 software (Leica). Quantification of nuclear p-JNK intensity was performed using Cell Profiler Software. After background correction, nuclei (DAPI) were defined as primary objects. pJNK signal intensity in nuclei was quantified as the mean intensity inside the primary object boundaries. pJNK intensity quantification was performed on at least 30 nuclei per experimental condition from four independent experiments.

Statistics. Graphs represent mean + SEM of at least three independent experiments, and statistical analysis was performed using a two-tailed Student's *t* test unless otherwise indicated in the figure legend. *, $P < 0.05$; **, $P < 0.01$; ***, $P < 0.001$.

We thank the Cancer Genome Atlas consortium for providing access to unpublished datasets and Carmelo Carlo Stella for sharing DLBCL cell lines. Methylation array experiments were performed at the USC Epigenome Center core facility, Los Angeles, and RNA sequencing was performed at the Functional Genomics Center Zürich. We are grateful to Raffaella Santoro and Sandra Frommel for help with chromatin immunoprecipitations.

This work was supported by grants from the Swiss Cancer League (KFS-02640-08-2010) and the Cancer League of the Canton of Zürich to A. Müller. M.D. Robinson acknowledges financial support from the Swiss National Science Foundation (project grant 143883) and from the European Commission through the seventh Framework Collaborative Project RADIANT (Grant Agreement Number: 305626). A. Tzankov is supported by the Foundation for the Fight against Cancer, Zürich.

The authors declare no competing financial interests.

Submitted: 16 October 2014
Accepted: 19 March 2015

REFERENCES

Agrelo, R., F. Setien, J. Espada, M.J. Artiga, M. Rodriguez, A. Pérez-Rosado, A. Sanchez-Aguilera, M.F. Fraga, M.A. Piris, and M. Esteller. 2005. Inactivation of the lamin A/C gene by CpG island promoter hypermethylation in hematologic malignancies, and its association with poor survival in nodal diffuse large B-cell lymphoma. *J. Clin. Oncol.* 23:3940–3947. http://dx.doi.org/10.1200/JCO.2005.11.650

Alizadeh, A.A., M.B. Eisen, R.E. Davis, C. Ma, I.S. Lossos, A. Rosenwald, J.C. Boldrick, H. Sabet, T. Tran, X. Yu, et al. 2000. Distinct types of diffuse large B-cell lymphoma identified by gene expression profiling. *Nature.* 403:503–511. http://dx.doi.org/10.1038/35000501

Anders, S., D.J. McCarthy, Y. Chen, M. Okoniewski, G.K. Smyth, W. Huber, and M.D. Robinson. 2013. Count-based differential expression analysis of RNA sequencing data using R and Bioconductor. *Nat. Protoc.* 8:1765–1786. http://dx.doi.org/10.1038/nprot.2013.099

Asmar, F., V. Punj, J. Christensen, M.T. Pedersen, A. Pedersen, A.B. Nielsen, C. Hother, U. Ralfkiaer, P. Brown, E. Ralfkiaer, et al. 2013. Genome-wide profiling identifies a DNA methylation signature that associates with TET2 mutations in diffuse large B-cell lymphoma. *Haematologica.* 98:1912–1920. http://dx.doi.org/10.3324/haematol.2013.088740

Balko, J.M., R.S. Cook, D.B. Vaught, M.G. Kuba, T.W. Miller, N.E. Bhola, M.E. Sanders, N.M. Granja-Ingram, J.J. Smith, I.M. Meszoely, et al. 2012. Profiling of residual breast cancers after neoadjuvant chemotherapy identifies DUSP4 deficiency as a mechanism of drug resistance. *Nat. Med.* 18:1052–1059. http://dx.doi.org/10.1038/nm.2795

Balko, J.M., L.J. Schwarz, N.E. Bhola, R. Kurupi, P. Owens, T.W. Miller, H. Gómez, R.S. Cook, and C.L. Arteaga. 2013. Activation of MAPK pathways due to DUSP4 loss promotes cancer stem cell-like phenotypes in basal-like breast cancer. *Cancer Res.* 73:6346–6358. http://dx.doi.org/10.1158/0008-5472.CAN-13-1385

Baudis, M., and M.L. Cleary. 2001. Progenetix.net: an online repository for molecular cytogenetic aberration data. *Bioinformatics.* 17:1228–1229. http://dx.doi.org/10.1093/bioinformatics/17.12.1228

Bethge, N., H. Honne, K. Andresen, V. Hilden, G. Trøen, K. Liestøl, H. Holte, J. Delabie, G.E. Lind, and E.B. Smeland. 2014. A gene panel, including LRP12, is frequently hypermethylated in major types of B-cell lymphoma. *PLoS ONE.* 9:e104249. http://dx.doi.org/10.1371/journal.pone.0104249

Boukhiar, M.A., C. Roger, J. Tran, R. Gressin, A. Martin, F. Ajchenbaum-Cymbalista, N. Varin-Blank, D. Ledoux, and F. Baran-Marszak. 2013. Targeting early B-cell receptor signaling induces apoptosis in leukemic mantle cell lymphoma. *Exp. Hematol. Oncol.* 2:4. http://dx.doi.org/10.1186/2162-3619-2-4

Cagnol, S., and N. Rivard. 2013. Oncogenic KRAS and BRAF activation of the MEK/ERK signaling pathway promotes expression of dual-specificity phosphatase 4 (DUSP4/MKP2) resulting in nuclear ERK1/2 inhibition. *Oncogene.* 32:564–576. http://dx.doi.org/10.1038/onc.2012.88

Ceribelli, M., P.N. Kelly, A.L. Shaffer, G.W. Wright, W. Xiao, Y. Yang, L.A. Mathews Griner, R. Guha, P. Shinn, J.M. Keller, et al. 2014. Blockade of oncogenic IκB kinase activity in diffuse large B-cell lymphoma by bromodomain and extraterminal domain protein inhibitors. *Proc. Natl. Acad. Sci. USA.* 111:11365–11370. http://dx.doi.org/10.1073/pnas.1411701111

Chambwe, N., M. Kormaksson, H. Geng, S. De, F. Michor, N.A. Johnson, R.D. Morin, D.W. Scott, L.A. Godley, R.D. Gascoyne, et al. 2014. Variability in DNA methylation defines novel epigenetic subgroups of DLBCL associated with different clinical outcomes. *Blood.* 123:1699–1708. http://dx.doi.org/10.1182/blood-2013-07-509885

Clozel, T., S. Yang, R.L. Elstrom, W. Tam, P. Martin, M. Kormaksson, S. Banerjee, A. Vasanthakumar, B. Culjkovic, D.W. Scott, et al. 2013. Mechanism-based epigenetic chemosensitization therapy of diffuse large B-cell lymphoma. *Cancer Discov.* 3:1002–1019. http://dx.doi.org/10.1158/2159-8290.CD-13-0117

Craig, V.J., S.B. Cogliatti, J. Imig, C. Renner, S. Neuenschwander, H. Rehrauer, R. Schlapbach, S. Dirnhofer, A. Tzankov, and A. Müller. 2011a. Myc-mediated repression of microRNA-34a promotes high-grade transformation of B-cell lymphoma by dysregulation of FoxP1. *Blood.* 117:6227–6236. http://dx.doi.org/10.1182/blood-2010-10-312231

Craig, V.J., S.B. Cogliatti, H. Rehrauer, T. Wündisch, and A. Müller. 2011b. Epigenetic silencing of microRNA-203 dysregulates ABL1 expression and drives Helicobacter-associated gastric lymphomagenesis. *Cancer Res.* 71:3616–3624. http://dx.doi.org/10.1158/0008-5472.CAN-10-3907

Cultrera, J.L., and S.M. Dalia. 2012. Diffuse large B-cell lymphoma: current strategies and future directions. *Cancer Contr.* 19:204–213.

Davis, R.E., V.N. Ngo, G. Lenz, P. Tolar, R.M. Young, P.B. Romesser, H. Kohlhammer, L. Lamy, H. Zhao, Y. Yang, et al. 2010. Chronic active B-cell-receptor signalling in diffuse large B-cell lymphoma. *Nature.* 463:88–92. http://dx.doi.org/10.1038/nature08638

De, S., R. Shaknovich, M. Riester, O. Elemento, H. Geng, M. Kormaksson, Y. Jiang, B. Woolcock, N. Johnson, J.M. Polo, et al. 2013. Aberration in DNA methylation in B-cell lymphomas has a complex origin and increases with disease severity. *PLoS Genet.* 9:e1003137. http://dx.doi.org/10.1371/journal.pgen.1003137

Dhanak, D., and P. Jackson. 2014. Development and classes of epigenetic drugs for cancer. *Biochem. Biophys. Res. Commun.* 455:58–69. http://dx.doi.org/10.1016/j.bbrc.2014.07.006

Esteller, M., G. Gaidano, S.N. Goodman, V. Zagonel, D. Capello, B. Botto, D. Rossi, A. Gloghini, U. Vitolo, A. Carbone, et al. 2002. Hypermethylation of the DNA repair gene O^6-methylguanine DNA methyltransferase and survival of patients with diffuse large B-cell lymphoma. *J. Natl. Cancer Inst.* 94:26–32. http://dx.doi.org/10.1093/jnci/94.1.26

Fey, D., D.R. Croucher, W. Kolch, and B.N. Kholodenko. 2012. Crosstalk and signaling switches in mitogen-activated protein kinase cascades. *Front. Physiol.* 3:355. http://dx.doi.org/10.3389/fphys.2012.00355

Fraga, M.F., M. Berdasco, E. Ballestar, S. Ropero, P. Lopez-Nieva, L. Lopez-Serra, J.I. Martín-Subero, M.J. Calasanz, I. Lopez de Silanes, F. Setien, et al. 2008. Epigenetic inactivation of the Groucho homologue gene *TLE1* in hematologic malignancies. *Cancer Res.* 68:4116–4122. http://dx.doi.org/10.1158/0008-5472.CAN-08-0085

Frommer, M., L.E. McDonald, D.S. Millar, C.M. Collis, F. Watt, G.W. Grigg, P.L. Molloy, and C.L. Paul. 1992. A genomic sequencing protocol that yields a positive display of 5-methylcytosine residues in individual DNA strands. *Proc. Natl. Acad. Sci. USA.* 89:1827–1831. http://dx.doi.org/10.1073/pnas.89.5.1827

Guan, H., L. Xie, F. Leithäuser, L. Flossbach, P. Möller, T. Wirth, and A. Ushmorov. 2010. KLF4 is a tumor suppressor in B-cell non-Hodgkin lymphoma and in classic Hodgkin lymphoma. *Blood.* 116:1469–1478. http://dx.doi.org/10.1182/blood-2009-12-256446

Gupta, S., T. Barrett, A.J. Whitmarsh, J. Cavanagh, H.K. Sluss, B. Dérijard, and R.J. Davis. 1996. Selective interaction of JNK protein kinase isoforms with transcription factors. *EMBO J.* 15:2760–2770.

Isaacson, P.G., and M.Q. Du. 2004. MALT lymphoma: from morphology to molecules. *Nat. Rev. Cancer.* 4:644–653. http://dx.doi.org/10.1038/nrc1409

Jemaà, M., I. Vitale, O. Kepp, F. Berardinelli, L. Galluzzi, L. Senovilla, G. Mariño, S.A. Malik, S. Rello-Varona, D. Lissa, et al. 2012. Selective killing of p53-deficient cancer cells by SP600125. *EMBO Mol. Med.* 4:500–514. http://dx.doi.org/10.1002/emmm.201200228

Kim, D., G. Pertea, C. Trapnell, H. Pimentel, R. Kelley, and S.L. Salzberg. 2013. TopHat2: accurate alignment of transcriptomes in the presence of insertions, deletions and gene fusions. *Genome Biol.* 14:R36. http://dx.doi.org/10.1186/gb-2013-14-4-r36

Kumaki, Y., M. Oda, and M. Okano. 2008. QUMA: quantification tool for methylation analysis. *Nucleic Acids Res.* 36:W170-W175. http://dx.doi.org/10.1093/nar/gkn294

Lawrence, M., W. Huber, H. Pagès, P. Aboyoun, M. Carlson, R. Gentleman, M.T. Morgan, and V.J. Carey. 2013. Software for computing and annotating genomic ranges. *PLOS Comput. Biol.* 9:e1003118. http://dx.doi.org/10.1371/journal.pcbi.1003118

Lenz, G., I. Nagel, R. Siebert, A.V. Roschke, W. Sanger, G.W. Wright, S.S. Dave, B. Tan, H. Zhao, A. Rosenwald, et al. 2007. Aberrant immunoglobulin class switch recombination and switch translocations in activated B cell-like diffuse large B cell lymphoma. *J. Exp. Med.* 204:633–643. http://dx.doi.org/10.1084/jem.20062041

Lenz, G., G. Wright, S.S. Dave, W. Xiao, J. Powell, H. Zhao, W. Xu, B. Tan, N. Goldschmidt, J. Iqbal, et al. Lymphoma/Leukemia Molecular Profiling Project. 2008. Stromal gene signatures in large-B-cell lymphomas. *N. Engl. J. Med.* 359:2313–2323. http://dx.doi.org/10.1056/NEJMoa0802885

Leventaki, V., E. Drakos, M. Karanikou, K. Psatha, P. Lin, E. Schlette, A. Eliopoulos, T.P. Vassilakopoulos, H. Papadaki, E. Patsouris, et al. 2014. c-JUN N-terminal kinase (JNK) is activated and contributes to tumor cell proliferation in classical Hodgkin lymphoma. *Hum. Pathol.* 45:565–572. http://dx.doi.org/10.1016/j.humpath.2013.10.024

Li, Y., H. Nagai, T. Ohno, M. Yuge, S. Hatano, E. Ito, N. Mori, H. Saito, and T. Kinoshita. 2002. Aberrant DNA methylation of $p57^{KIP2}$ gene in the promoter region in lymphoid malignancies of B-cell phenotype. *Blood.* 100:2572–2577. http://dx.doi.org/10.1182/blood-2001-11-0026

Martinez-Delgado, B., J. Fernandez-Piqueras, M.J. Garcia, E. Arranz, J. Gallego, C. Rivas, M. Robledo, and J. Benitez. 1997. Hypermethylation of a 5′ CpG island of p16 is a frequent event in non-Hodgkin's lymphoma. *Leukemia.* 11:425–428. http://dx.doi.org/10.1038/sj.leu.2400579

Mathews Griner, L.A., R. Guha, P. Shinn, R.M. Young, J.M. Keller, D. Liu, I.S. Goldlust, A. Yasgar, C. McKnight, M.B. Boxer, et al. 2014. High-throughput combinatorial screening identifies drugs that cooperate with ibrutinib to kill activated B-cell-like diffuse large B-cell lymphoma cells. *Proc. Natl. Acad. Sci. USA.* 111:2349–2354. http://dx.doi.org/10.1073/pnas.1311846111

Matsuda, K., A. Sato, M. Okada, K. Shibuya, S. Seino, K. Suzuki, E. Watanabe, Y. Narita, S. Shibui, T. Kayama, and C. Kitanaka. 2012. Targeting JNK for therapeutic depletion of stem-like glioblastoma cells. *Sci. Rep.* 2:516. http://dx.doi.org/10.1038/srep00516

Meyer, P.N., K. Fu, T.C. Greiner, L.M. Smith, J. Delabie, R.D. Gascoyne, G. Ott, A. Rosenwald, R.M. Braziel, E. Campo, et al. 2011. Immunohistochemical methods for predicting cell of origin and survival in patients with diffuse large B-cell lymphoma treated with rituximab. *J. Clin. Oncol.* 29:200–207. http://dx.doi.org/10.1200/JCO.2010.30.0368

Muenst, S., S. Hoeller, N. Willi, S. Dirnhofera, and A. Tzankov. 2010. Diagnostic and prognostic utility of PD-1 in B cell lymphomas. *Dis. Markers.* 29:47–53. http://dx.doi.org/10.1155/2010/404069

Pasqualucci, L., and R. Dalla-Favera. 2014. SnapShot: diffuse large B cell lymphoma. *Cancer Cell.* 25:132: e1. http://dx.doi.org/10.1016/j.ccr.2013.12.012

Price, M.E., A.M. Cotton, L.L. Lam, P. Farré, E. Emberly, C.J. Brown, W.P. Robinson, and M.S. Kobor. 2013. Additional annotation enhances potential for biologically-relevant analysis of the Illumina Infinium HumanMethylation450 BeadChip array. *Epigenetics Chromatin.* 6:4. http://dx.doi.org/10.1186/1756-8935-6-4

Robinson, C.J., C.M. Sloss, and R. Plevin. 2001. Inactivation of JNK activity by mitogen-activated protein kinase phosphatase-2 in EAhy926 endothelial cells is dependent upon agonist-specific JNK translocation to the nucleus. *Cell. Signal.* 13:29–41. http://dx.doi.org/10.1016/S0898-6568(00)00121-2

Roschewski, M., L.M. Staudt, and W.H. Wilson. 2014. Diffuse large B-cell lymphoma—treatment approaches in the molecular era. *Nat. Rev. Clin. Oncol.* 11:12–23. http://dx.doi.org/10.1038/nrclinonc.2013.197

Rosenwald, A., G. Wright, K. Leroy, X. Yu, P. Gaulard, R.D. Gascoyne, W.C. Chan, T. Zhao, C. Haioun, T.C. Greiner, et al. 2003. Molecular diagnosis of primary mediastinal B cell lymphoma identifies a clinically favorable subgroup of diffuse large B cell lymphoma related to Hodgkin lymphoma. *J. Exp. Med.* 198:851–862. http://dx.doi.org/10.1084/jem.20031074

Schmitz, R., R.M. Young, M. Ceribelli, S. Jhavar, W. Xiao, M. Zhang, G. Wright, A.L. Shaffer, D.J. Hodson, E. Buras, et al. 2012. Burkitt lymphoma pathogenesis and therapeutic targets from structural and functional genomics. *Nature.* 490:116–120. http://dx.doi.org/10.1038/nature11378

Schneider, C., L. Pasqualucci, and R. Dalla-Favera. 2011. Molecular pathogenesis of diffuse large B-cell lymphoma. *Semin. Diagn. Pathol.* 28:167–177. http://dx.doi.org/10.1053/j.semdp.2011.04.001

Shaffer, A.L. III, R.M. Young, and L.M. Staudt. 2012. Pathogenesis of human B cell lymphomas. *Annu. Rev. Immunol.* 30:565–610. http://dx.doi.org/10.1146/annurev-immunol-020711-075027

Shaknovich, R., H. Geng, N.A. Johnson, L. Tsikitas, L. Cerchietti, J.M. Greally, R.D. Gascoyne, O. Elemento, and A. Melnick. 2010. DNA methylation signatures define molecular subtypes of diffuse large B-cell lymphoma. *Blood.* 116:e81–e89. http://dx.doi.org/10.1182/blood-2010-05-285320

Shen, Y.H., J. Godlewski, J. Zhu, P. Sathyanarayana, V. Leaner, M.J. Birrer, A. Rana, and G. Tzivion. 2003. Cross-talk between JNK/SAPK and ERK/MAPK pathways: sustained activation of JNK blocks ERK activation by mitogenic factors. *J. Biol. Chem.* 278:26715–26721. http://dx.doi.org/10.1074/jbc.M303264200

Teixeira, C., S.L. Stang, Y. Zheng, N.S. Beswick, and J.C. Stone. 2003. Integration of DAG signaling systems mediated by PKC-dependent phosphorylation of RasGRP3. *Blood.* 102:1414–1420. http://dx.doi.org/10.1182/blood-2002-11-3621

Visco, C., Y. Li, Z.Y. Xu-Monette, R.N. Miranda, T.M. Green, Y. Li, A. Tzankov, W. Wen, W.M. Liu, B.S. Kahl, et al. 2012. Comprehensive gene expression profiling and immunohistochemical studies support application of immunophenotypic algorithm for molecular subtype classification in diffuse large B-cell lymphoma: a report from the International DLBCL Rituximab-CHOP Consortium Program Study. *Leukemia.* 26:2103–2113. http://dx.doi.org/10.1038/leu.2012.83

Volk, A., J. Li, J. Xin, D. You, J. Zhang, X. Liu, Y. Xiao, P. Breslin, Z. Li, W. Wei, et al. 2014. Co-inhibition of NF-κB and JNK is synergistic in TNF-expressing human AML. *J. Exp. Med.* 211:1093–1108. http://dx.doi.org/10.1084/jem.20130990

Waha, A., J. Felsberg, W. Hartmann, A. von dem Knesebeck, T. Mikeska, S. Joos, M. Wolter, A. Koch, P.S. Yan, E. Endl, et al. 2010. Epigenetic downregulation of mitogen-activated protein kinase phosphatase MKP-2 relieves its growth suppressive activity in glioma cells. *Cancer Res.* 70:1689–1699. http://dx.doi.org/10.1158/0008-5472.CAN-09-3218

Wang, M., C. Atayar, S. Rosati, A. Bosga-Bouwer, P. Kluin, and L. Visser. 2009. JNK is constitutively active in mantle cell lymphoma: cell cycle deregulation and polyploidy by JNK inhibitor SP600125. *J. Pathol.* 218:95–103. http://dx.doi.org/10.1002/path.2521